

Organization of cortico-cortical pathways supporting memory retrieval across subregions of the left ventrolateral prefrontal cortex

Jennifer Barredo,^{1,3} Timothy D. Verstynen,^{4,5} and David Badre^{2,3}

¹Department of Neuroscience, Brown University, Providence, Rhode Island; ²Department of Cognitive, Linguistic, and Psychological Sciences, Brown University, Providence, Rhode Island; ³Brown Institute for Brain Sciences, Brown University, Providence, Rhode Island; ⁴Department of Psychology, Carnegie Mellon University, Pittsburgh, Pennsylvania; and ⁵Center for the Neural Basis of Cognition, Carnegie Mellon University, Pittsburgh, Pennsylvania

Submitted 22 February 2016; accepted in final form 2 June 2016

Barredo J, Verstynen TD, Badre D. Organization of cortico-cortical pathways supporting memory retrieval across subregions of the left ventrolateral prefrontal cortex. *J Neurophysiol* 116: 920–937, 2016. First published June 8, 2016; doi:10.1152/jn.00157.2016.—Functional magnetic resonance imaging (fMRI) evidence indicates that different subregions of ventrolateral prefrontal cortex (VLPFC) participate in distinct cortical networks. These networks have been shown to support separable cognitive functions: anterior VLPFC [inferior frontal gyrus (IFG) pars orbitalis] functionally correlates with a ventral fronto-temporal network associated with top-down influences on memory retrieval, while mid-VLPFC (IFG pars triangularis) functionally correlates with a dorsal fronto-parietal network associated with postretrieval control processes. However, it is not known to what extent subregional differences in network affiliation and function are driven by differences in the organization of underlying white matter pathways. We used high-angular-resolution diffusion spectrum imaging and functional connectivity analysis in unanesthetized humans to address whether the organization of white matter connectivity differs between subregions of VLPFC. Our results demonstrate a ventral-dorsal division within IFG. Ventral IFG as a whole connects broadly to lateral temporal cortex. Although several different individual white matter tracts form connections between ventral IFG and lateral temporal cortex, functional connectivity analysis of fMRI data indicates that these are part of the same ventral functional network. By contrast, across subdivisions, dorsal IFG was connected with the midfrontal gyrus and correlated as a separate dorsal functional network. These qualitative differences in white matter organization within larger macroanatomical subregions of VLPFC support prior functional distinctions among these regions observed in task-based and functional connectivity fMRI studies. These results are consistent with the proposal that anatomical connectivity is a crucial determinant of systems-level functional organization of frontal cortex and the brain in general.

ventrolateral prefrontal cortex; anatomical connectivity; functional connectivity; prefrontal organization; diffusion spectrum imaging

NEW & NOTEWORTHY

High-angular-resolution diffusion imaging, deterministic tractography, and functional connectivity were used to analyze the connectivity of the human ventrolateral prefrontal cortex (VLPFC). Evidence is provided for separate ventral and dorsal connectivity zones within VLPFC. Data suggest that dorsal VLPFC as a whole is part of a general cognitive control network, in contrast to earlier work

Address for reprint requests and other correspondence: J. Barredo, Providence VA Medical Ctr., Research/Bldg. #32, Providence, RI 02908 (e-mail: jennifer.barredo@va.gov).

suggesting that caudal VLPFC supports cognitive control whereas mid- to anterior VLPFC is functionally important for language and semantic processing.

THE LEFT VENTROLATERAL PREFRONTAL CORTEX (VLPFC) has long been known to play a role in both language and memory function (reviewed in Badre and Wagner 2007; Fedorenko and Thompson-Schill 2014; Hagoort 2013; Spaniol et al. 2009). Cognitive neuroscience investigations suggest that VLPFC subregions are functionally heterogeneous (Badre et al. 2005; Barredo et al. 2015; Gabrieli et al. 1998; Gold et al. 2006; Wagner et al. 2001), yet the underlying characteristics imparting these functional distinctions are underspecified.

The left VLPFC refers to lateral inferior frontal gyrus (IFG) anterior to premotor cortex and extending to the ventral bank of the inferior frontal sulcus. Conventionally, VLPFC is divided into three macroanatomical subdivisions. At the caudal extent, pars opercularis occupies IFG between the rostral bank of precentral sulcus and the anterior ascending limb of the lateral sulcus. Pars triangularis is rostral to opercularis and extends to the horizontal ramus of the lateral sulcus. Pars orbitalis, the most rostral IFG subregion, extends into caudal lateral orbital gyrus. Orbitalis, triangularis, and opercularis also differ roughly in cytoarchitecture, approximating Brodmann's areas 47, 45, and 44, respectively (Petrides and Pandya 2002).

Evidence from functional magnetic resonance imaging (fMRI) indicates that VLPFC subregions participate in distinct functions during memory retrieval (Badre et al. 2005; Barredo et al. 2015; Gold et al. 2006; Race et al. 2008; Wagner et al. 2001). Anterior VLPFC (aVLPFC, ~orbitalis) is typically engaged by tasks demanding control over memory access, whereas mid-VLPFC (~triangularis) is engaged by “postretrieval” control demands (Badre et al. 2005; Barredo et al. 2015), such as those related to monitoring, decision making, and response selection. Recently, an fMRI experiment demonstrated that when aVLPFC and mid-VLPFC were defined on the basis of their engagement during these respective memory control processes, they participated in separate functional connectivity networks. Using functional connectivity MRI analysis, Barredo et al. (2015) showed that aVLPFC and other temporal regions [anterior temporal cortex (aTC), anterior parahippocampal gyrus, hippocampus] exhibited activation characteristic of controlled retrieval and demonstrated greater functional connectivity with each other than with regions outside of this network. By contrast, mid-VLPFC and dorso-lateral frontal and parietal regions [dorsolateral prefrontal cortex (DLPFC), mid-frontal gyrus (MFG), intraparietal sulcus

(IPS)] were functionally related to postretrieval control processes and comprised a separate functional connectivity network. These “dorsal pathway” and “ventral pathway” networks were largely nonoverlapping, with the exception of aVLPFC, which correlated with both networks.

The results from Barredo et al. (2015) suggest that prior observations of functional distinctions between aVLPFC and mid-VLPFC might reflect the participation of each region in separate functionally connected networks. Network models have demonstrated that direct and indirect structural connections are predictive of functional connectivity networks (Honey et al. 2009). As such, the anatomical connectivity of VLPFC subregions may define the functional organization of VLPFC more precisely than the common macroanatomical divisions. The present study sought to examine the relationship between specific white matter pathways to dissociable functional connectivity networks implicated in memory retrieval (Alm et al. 2016; Barredo et al. 2015).

Previous investigations using anatomical tracers in nonhuman primates and diffusion imaging tractography in humans suggest that the ventral white matter may serve as the principal anatomical pathway that underlies the ventral functional pathway (reviewed in Barredo et al. 2015). Retrograde tracers have mapped temporal stem projections between macaque 47/12 and aTC (Barbas 1988; Carmichael and Price 1995; Petrides and Pandya 2002). Additionally, human dissections and tractography note that the uncinatus fasciculus connects frontal and anterior temporal lobes via the temporal stem (Catani and Thibaut de Schotten 2008; Kier et al. 2004; Martino et al. 2011). Furthermore, the extreme fiber capsule system (EFCS) that connects VLPFC to superior temporal gyrus (STG) via the temporal stem provides an additional anatomical pathway between these regions as demonstrated via tracer work in monkeys (Petrides and Pandya 1988, 2009) and human diffusion imaging (Frey et al. 2008; Makris and Pandya 2009). Given these findings, we predicted that VLPFC subregions implicated in the ventral functional pathway involved in memory retrieval (Barredo et al. 2015) will project to aTC through the ventral white matter containing these anatomical pathways.

Second, we predict that the mid-VLPFC will exhibit white matter connectivity with the dorsal pathway (Barredo et al. 2015). Indeed, previous human tractography investigations corroborate observations of direct VLPFC-parietal fibers via the superior longitudinal fasciculus (SLF) and/or arcuate fasciculus (Catani et al. 2005; Frey et al. 2008; Makris and Pandya 2009; Martino et al. 2011; Thibaut de Schotten et al. 2012) reported in the macaque (Petrides and Pandya 1999). We predict that extrinsic connectivity with this pathway should be characteristic of VLPFC regions, likely mid-VLPFC, functionally linked to postretrieval operations.

Here we used high-angular-resolution diffusion spectrum imaging (DSI) and fiber tractography to test whether human white matter connectivity supports the previously observed functional dissociation between the ventral and dorsal functional pathways involved in memory retrieval (Barredo et al. 2015). Specifically, we addressed 1) whether the organization of white matter connectivity differs among the pars orbitalis, triangularis, and opercularis subregions of VLPFC and 2) whether finer anatomical connection-based parcellations of left VLPFC might be drawn based on extrinsic connectivity to

targets along the previously defined ventral and dorsal functional pathways.

METHODS

Participants

Nineteen participants (10 women, 9 men; mean age 26 yr) were included in the study. All participants were right-handed with no history of neurological or psychiatric diagnoses, use of medications with potential vascular or central nervous system effects, or contraindication for MRI. Participants were remunerated \$20/h. Written informed consent was obtained in accord with procedures approved by the Institutional Review Board of the Research Protections Office at Brown University. In two instances, the initial data set was too noisy; thus these participants were rescanned in a second session and included in the study. Four additional subjects were scanned but excluded because of movement, poor normalization, or excessive signal drop out in the temporal lobes. These participants were unavailable for rescanning.

MRI Image Acquisition

All data were acquired on a Siemens 3-T Tim Trio System with a 32-channel coil. For the 47-min DSI scan a 257-direction, twice-refocused spin-echo sequence with multiple q values was collected with a half-sphere sampling scheme (Weeden et al. 2005) ($2.4 \times 2.4 \times 2.4$ mm voxels, TR = 9,900 ms, TE = 157 ms, flip angle = 90° , b-max = $7,000$ s/mm²). fMRI data for resting-state analysis were collected after the DSI scan in one 6.2-min run of 124 volume acquisitions using a gradient-echo echo-planar sequence optimized for functional connectivity analysis (Van Dijk et al. 2010) ($3 \times 3 \times 3$ mm, TR = 3.0 s, TE = 30 ms, flip angle = 85° , 47 transverse slices, no skip, no dummy slices, fat saturation on). High-resolution T1-weighted anatomical images were collected for registration and visualization [multi-echo magnetization prepared rapid acquisition gradient echo (MEMPRAGE) $1.2 \times 1.2 \times 1.2$ mm voxels, 144 slices]. For full MEMPRAGE acquisition details, see van der Kouwe et al. (2008).

Diffusion Image Reconstruction

q-Space diffeomorphic reconstruction (Yeh and Tseng 2011), an application of the generalized q-sampling imaging reconstruction method to template space (Yeh et al. 2010), was implemented in DSI Studio. q-Space diffeomorphic reconstruction works by incorporating the nonlinear transformation into the reconstruction process itself (Yeh and Tseng 2011). Thus individual structure in diffusion geometry is accounted for during the reconstruction of models [i.e., orientation distribution functions (ODFs)] into a common space. Previous work has shown that this approach captures validated patterns of normative connectivity (Abhinav et al. 2014; Wang et al. 2013, 2016) while also accounting for meaningful individual differences in white matter pathways (Jarbo and Verstynen 2015; Verstynen 2014). Images were masked to eliminate voxels outside of the brain from reconstructions. A diffusion ODF was reconstructed from the 257 discrete sampling directions of the DSI scan (8-fold tessellation reconstruction) for each voxel. The ODF reconstruction was immediately projected into template Montreal Neurological Institute (MNI) space with a nonlinear registration routine (ICBM-152 space template regularization, 16 nonlinear iterations), and voxels were upsampled to a 1-mm³ resolution. The quantitative anisotropy (QA; Yeh et al. 2010) and orientation of the first five peaks in the ODF were then identified and used for deterministic fiber tractography (see below; Yeh et al. 2013).

Region of Interest Definition and Tracking of Fiber Streamlines

Cortical regions of interest (ROIs) used for tracking of fiber streamlines were adapted from the SRI24/TZO Atlas (Rohlfing et al. 2010), a probabilistic implementation of the Automated Anatomical Labeling (AAL) definitions of Tzourio-Mazoyer et al. (2002). The boundaries of all ROIs were expanded by one voxel and smoothed to account for distortions and partial-volume effects during registration to diffusion images. See Table 1 for a list of all ROI masks, abbreviations for regions, and the predicted pathway (dorsal or ventral) in which they were grouped. During fiber streamline tracking, ROIs could serve as seed and/or target regions. The term “seed region” is used to denote ROIs from which fiber streamline tracking was initiated, while “target regions” designate regions where the density and topography of fiber streamline end points were investigated. See Fig. 1 for views of the ventral and dorsal white matter ROIs and Fig. 2 for an illustration of the cortical ROIs.

Deterministic fiber streamline tracking was performed with DSI Studio processing software (Yeh et al. 2013). A ROI-based approach was used for streamline tracking. Two white matter ROIs (Fig. 1, A and B) were used to track streamlines connecting VLPFC with the parietal and temporal cortices, a mask of the white matter between ventral IFG and temporal cortex guided by the descriptions of the temporal stem (Kier et al. 2004) and the EFCS (Makris and Pandya 2009) and a mask of SLF/arcuate based on the JHU Matter Atlas (Wakana et al. 2004). Spatially intermediate seed ROIs were used to reduce the false-negative tractography results observed with the ROI seed-to-target approach (Conturo et al. 1999). Seed-to-ROI tracking may produce slightly different results because of a spatial bias toward the reconstruction of streamlines proximal to the seed. Thus we seeded the white matter between ROI pairs of interest in an effort to limit this bias. To limit the number of false-positive streamlines (e.g., streamlines that pass through but do not terminate in target regions or are outside of the brain), streamlines were only kept if they had end points in a VLPFC target region and in the cortical target region. This requirement eliminates streamlines that simply pass through each region.

Each tracking attempt was initiated from a random position and direction within the seed mask and progressed in 0.5-mm steps. Fiber streamlines were excluded if 1) the normalized QA (NQA; maximum QA within subject scaled to 1.0) dropped below a subject-specific threshold (range: 0.03–0.06); 2) the streamline exceeded the pathway- or region-specific maximum turning angle (range: 45–70°); 3) the streamline extended beyond the target-specific tract length thresh-

old (80–140 mm); or 4) streamline length was shorter than the minimum target-specific tract length threshold (5–60 mm). Fiber streamlines were additionally smoothed such that each incoming directional estimate was weighted by a percentage of the previous directional estimate (e.g., if the smoothing value = 0.60, the incoming directional estimate is 60% dependent on the previous estimate). For any individual seed-to-target pair, the number of streamline attempts were equal to the number of voxels in the seed region \times 10; thus the number of tracking opportunities was scaled to the volume of the tracking seed. For a summary of pathway-specific streamline tracking parameters, see Table 1.

Two fiber tracking parameters, the NQA threshold and the fiber smoothing parameter, were subject specific. Subject-specific NQA and smoothing values were used to equalize the number of fiber streamlines generated by tracking attempts across subjects in an effort to account for differences in signal-to-noise ratio occurring between different scanning sessions. Care was taken to adjust these parameters in an unbiased way. Starting from the NQA level maximizing signal to noise within each participant according to Otsu's method (Otsu 1979), the NQA was lowered and the smoothing parameter was adjusted until seeding produced a given number of fiber streamlines. This step equalized the number of fiber streamlines generated from the ventral, dorsal, and VLPFC seed masks across subjects. Once set, they were not adjusted again. This method has been used in other DSI studies to normalize signal to noise (Jarbo et al. 2012; Verstynen et al. 2011, 2012). The resulting signal-to-noise ratio-normalized parameters were then used in subsequent seed-to-target fiber tracking. Subsequent within-pathway tracking attempts applied the NQA and smoothing parameters generated from the equalization step regardless of the end-point masks used for ROI-to-ROI tracking. For subject-specific parameters see Table 2.

A slightly different procedure was used to investigate IFG-to-MFG anatomical connectivity. Here, IFG subregions were treated as seeds given their close proximity to the MFG. For IFG-MFG fiber tracking, we imposed a minimum streamline length of at least 5 mm. This minimum length requirement was selected to limit the number of false-positive end points despite the close proximity of these regions. This length requirement is larger than the overlap of the VLPFC and MFG ROIs and conservatively offsets the proximity bias while excluding some valid U-fiber streamlines. To verify that our length requirement was sufficient to offset any spatial smoothness that might bias tractography, an end-point smoothness analysis was conducted. Average smoothness in the x , y , and z dimensions of 1.9, 1.9, and

Table 1. Summary of regions of interest outside of VLPFC

Structure	Abbreviation	Path Seed	Min. Length, mm	Max. Length, mm	Max. Angle, °
Sup. temporal pole	sPole	Ventral	5	80	65
Mid. temporal pole	mPole	Ventral	5	80	65
Sup. temporal gyrus	STG	Ventral	5	80	65
		Dorsal	20	120	65
Mid. temporal gyrus	MTG	Ventral	5	80	65
		Dorsal	20	120	65
Inf. temporal gyrus	ITG	Ventral	5	80	65
		Dorsal	20	120	65
Supramarginal gyrus	SMG	Ventral	50	180	70
		Dorsal	50	180	70
Angular gyrus	AG	Ventral	50	180	70
		Dorsal	50	180	70
Inf. parietal lobule	IPL	Ventral	50	180	70
		Dorsal	50	180	70
Mid. frontal gyrus	MFG	U fibers	5	45	45
Sup. longitudinal fasciculus	SLF	Dorsal	N/A	N/A	N/A
Temporal stem	N/A	Ventral	N/A	N/A	N/A

Regions where N/A values are reported for tracking parameters are seed regions. Tracking parameters used with seed were variable and were dictated by the target region.

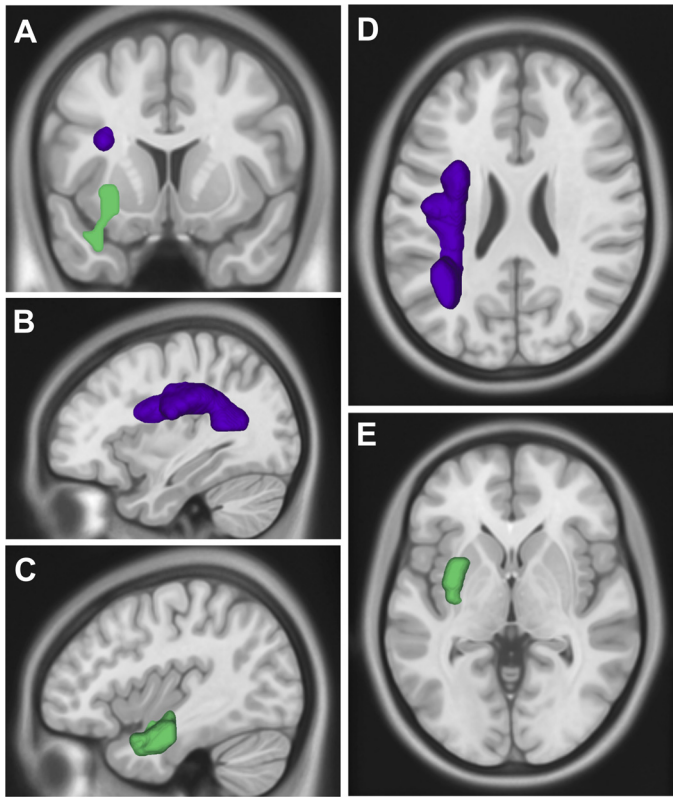


Fig. 1. Ventral and dorsal white matter seed ROIs. The ventral white matter seed region used to generate fiber streamlines between VLPFC and temporal cortex is pictured in green; the dorsal white matter seed used to generate fiber streamlines to temporal and parietal cortices is pictured in purple. Image orientations follow neurological convention. Slices were selected for maximum visibility; all ROIs are within boundaries of the skull. *A*: coronal view. *B*: sagittal view of the ventral white matter seed. *C*: sagittal view of the dorsal white matter seed. *D*: axial view of the ventral white matter seed. *E*: axial view of the dorsal white matter seed.

1.2 mm, respectively, indicated that end-point spread between the two regions was minimal.

Fiber Distribution and Density Analyses

All post hoc analyses of fiber streamline data described in the following sections were performed with in-house custom software written in MATLAB, as well as the NIFTI Tools (<https://www.mathworks.com/matlabcentral/mlc-downloads/downloads/submissions/8797/versions/28/download/zip>) image processing environment.

Fiber Streamline Distribution Analysis

The streamline distribution analysis compared the density of white matter connections between VLPFC subregions to target regions

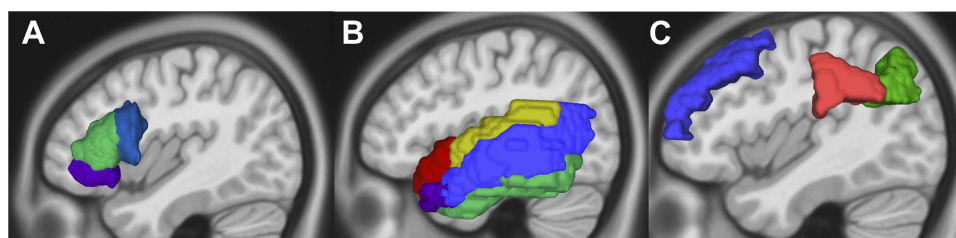


Fig. 2. Cortical ROIs. Pictures depict placement of cortical ROIs used as end-point targets for fiber tractography. Image orientation follows neurological convention. *A*: from left to right, pars orbitalis, pars triangularis, and pars opercularis. *B*: superior temporal pole (red), mid-temporal pole (purple), STG (yellow), MTG (blue), and ITG (green) ROIs. *C*: in frontal cortex MFG is pictured in blue, and in parietal cortex SMG is pictured in red and AG in green.

along the dorsal and ventral functional pathways. Target regions were excluded from this analysis if fiber tracking failed to produce >10 streamlines in at least half of our subjects. Omnibus between-subregion differences in the strength of connectivity were identified with a Friedman's nonparametric ANOVA; further nonparametric paired comparisons were tested with Wilcoxon signed-rank tests. All reported *P* values have undergone Bonferroni correction for multiple comparisons.

To illustrate the within-region topography of end points from dorsal and ventral pathway projections, a center of mass associated with each seed-target pair was calculated for each participant. The center of mass of fiber projection densities, *C*, was modeled as

$$C = \frac{\sum_{i=1}^V D_i X_i}{\sum_{i=1}^V D_i}$$

where *D_i* is the density of end points in each voxel *i* in the ROI mask, *V* is the number of voxels in the mask, and *X_i* is the Cartesian position of voxel *V_i* (Verstynen et al. 2012). All centers of mass are reported in MNI coordinates. These centers of mass were used in the topographic microorganization analysis outlined below.

Topographic Microorganization Analyses

In the microorganization analysis, we examined whether there are discrete anatomical end-point zones within VLPFC that preferentially project to either the dorsal or ventral functional pathways. The *x*, *y*, and *z* coordinates from the regional centers of mass for each subject (see *Fiber Streamline Distribution Analysis*) were entered into a repeated-measures multivariate analysis of variance (ANOVA) that compared the effect of pathway (dorsal or ventral) on relative end-point position. Follow-up paired comparisons were considered reliable if *P* < 0.05 after Bonferroni correction for multiple comparisons.

Functional Connectivity Analysis

The centers of mass from fiber streamlines that demonstrated reliable anatomical connectivity in the topographic analysis were used as seeds in a resting-state functional connectivity analysis to visualize associated resting-state networks.

The FreeSurfer surface-processing package (<http://freesurfer.net/>) was used to construct surface-space anatomical models and segmented tissue maps. These maps were used to define CSF and white matter in native space for the calculation of nuisance regressors included in subject-level models.

Functional data preprocessing was guided by the 1000 Functional Connectomes (http://fcon_1000.projects.nitrc.org/) data processing pipeline built with the AFNI (<http://afni.nimh.nih.gov/afni>) and FSL (<http://www.fmrib.ox.ac.uk/fsl/>) fMRI image processing packages. Functional images underwent slice-timing correction, motion correction, and band-pass filtering (0.009 < *f* < 0.08 Hz) in volume space. The processed images were then warped into anatomical surface space with AFNI's SUMA surface processing toolbox and were spatially smoothed in surface space with a 6-mm Gaussian kernel.

Table 2. Subject-specific streamline tracking parameters

Ventral-NQA	Ventral-Smooth	Dorsal-NQA	Dorsal-Smooth	IFG-NQA	IFG-Smooth
0.029	0.3	0.04	0.5	0.043	0.5
0.034	0.4	0.03	0.5	0.125	0.5
0.029	0.4	0.022	0.6	0.048	0.5
0.039	0.4	0.04	0.5	0.052	0.5
0.034	0.4	0.06	0.5	0.072	0.5
0.052	0.4	0.068	0.5	0.17	0.5
0.063	0.4	0.068	0.5	0.145	0.5
0.045	0.4	0.047	0.4	0.091	0.5
0.046	0.4	0.052	0.5	0.078	0.5
0.03	0.4	0.03	0.6	0.052	0.5
0.039	0.4	0.038	0.5	0.062	0.5
0.027	0.4	0.032	0.5	0.056	0.5
0.033	0.4	0.023	0.6	0.06	0.5
0.031	0.4	0.032	0.6	0.07	0.5
0.03	0.4	0.035	0.5	0.052	0.5
0.034	0.4	0.03	0.5	0.059	0.5
0.024	0.4	0.035	0.5	0.042	0.5
0.053	0.4	0.07	0.4	0.105	0.5
0.031	0.4	0.028	0.6	0.056	0.5

Statistical modeling was performed in surface rather than volume space to reduce spurious connectivity results due to spatial blurring across sulci. The motion parameters extracted during motion correction, time course of CSF signal and time course of white matter signal, were treated as regressors of no interest in subject-level models. In addition, to limit the influence of motion-related residual noise on our functional connectivity data (Power et al. 2014), time points where motion in any direction exceeded 0.3 mm or where voxel intensity exceeded three median average deviations in >0.01 voxels per volume were censored. These censored time points were also treated as regressors of no interest. One participant's functional connectivity data were excluded for censoring in excess of 10% of resting-state data. The resulting residuals from first-level regressions were extracted, mean-corrected, converted back to volume space, and then resampled to MNI space.

Seed-based functional connectivity assessed the correlation in signal between seed and target brain regions. Single voxels corresponding to fiber streamline centers of mass demonstrating reliable anatomical connectivity in the topographic analysis were used as seeds for correlation-based resting-state functional connectivity analysis. During first-level analysis, the signal time series over the session for each seed ROI was extracted, and Pearson's product moment correlations were used to compute the pairwise regional correlation between seed time courses and all other voxels in the volume. Resulting single-seed correlation maps were then converted to Z scores with Fisher's transformation. Individual subject's statistical maps were then entered into a second-level random effects analysis using a one-sample t -test against a contrast value of 0 at each voxel. Voxelwise group effects were considered reliable at $P < 0.05$ after false discovery rate (FDR) correction (Genovese et al. 2002) or $P < 0.001$; the more stringent of the two thresholds was always selected. To exclude small or singleton clusters, height-corrected maps were extent thresholded at 20 contiguous voxels. Visualizations of statistical maps are pictured with Caret software MRI imaging <http://brainvis.wustl.edu/wiki/index.php/Caret>: Download).

RESULTS

Tract Distribution Analyses

Temporal lobe connections via ventral vs. dorsal white matter. Axons from VLPFC neurons can connect with temporal cortex via a ventral route that enters the temporal cortex through the white matter of the temporal stem or EFCS (Catani

and Thibaut de Schotten 2008; Kier et al. 2004; Makris and Pandya 2009; Martino et al. 2011) or by a dorsal route that traverses the white matter between the frontal and parietal cortices containing the SLF and arcuate association fibers (Catani et al. 2005; Frey et al. 2008; Makris et al. 2005; Martino et al. 2011; Thibaut de Schotten et al. 2012). We first tested whether anatomical connectivity between VLPFC subregions and the temporal cortex was biased toward either pathway using temporal stem vs. SLF/arcuate seeds (Fig. 1, A and B).

The majority of fiber tracks connecting the pars orbitalis with temporal cortex did so via the ventral white matter (Wilcoxon signed-rank $Z = 3.82$, $p < 0.0001$; Fig. 3A), while tracks connecting opercularis with temporal cortex projected primarily through the dorsal white matter (Wilcoxon $Z = 3.82$, $P < 0.0001$; Fig. 3A). Triangularis connected to temporal lobe through both pathways (Fig. 3A), but there was a marginal bias (Wilcoxon $Z = 1.73$, $P = 0.08$) for the dorsal (median = 1,737 tracks) over the ventral white matter (median = 270 tracks).

Direct contrasts between VLPFC subregions further confirmed that pars orbitalis connections to the ventral white matter were denser than those of triangularis ($Z = 3.82$, $P < 0.005$) and opercularis ($Z = 3.82$, $P < 0.005$). There was no reliable difference in ventral white matter connectivity between triangularis and opercularis ($Z = 1.63$, $P < 0.10$).

The anatomical connectivity of pars opercularis with the dorsal white matter was greater than that of both orbitalis ($Z = 3.82$, $P < 0.001$) and triangularis ($Z = 3.78$, $P < 0.001$). Additionally, triangularis exhibited greater connectivity with the dorsal white matter than orbitalis ($Z = 3.53$, $P < 0.001$).

In summary, VLPFC connections to the temporal lobe via the dorsal white matter are organized along a connective gradient, such that rostral VLPFC (pars orbitalis) targets the temporal cortex primarily via the white matter of the temporal stem whereas more caudal VLPFC subregions (pars triangularis and opercularis) project to temporal cortex primarily via the white matter of the SLF and arcuate association fibers.

Distribution of connections across temporal subregions. We next tested the distribution of ventral white matter and dorsal white matter streamlines to subregions within the temporal

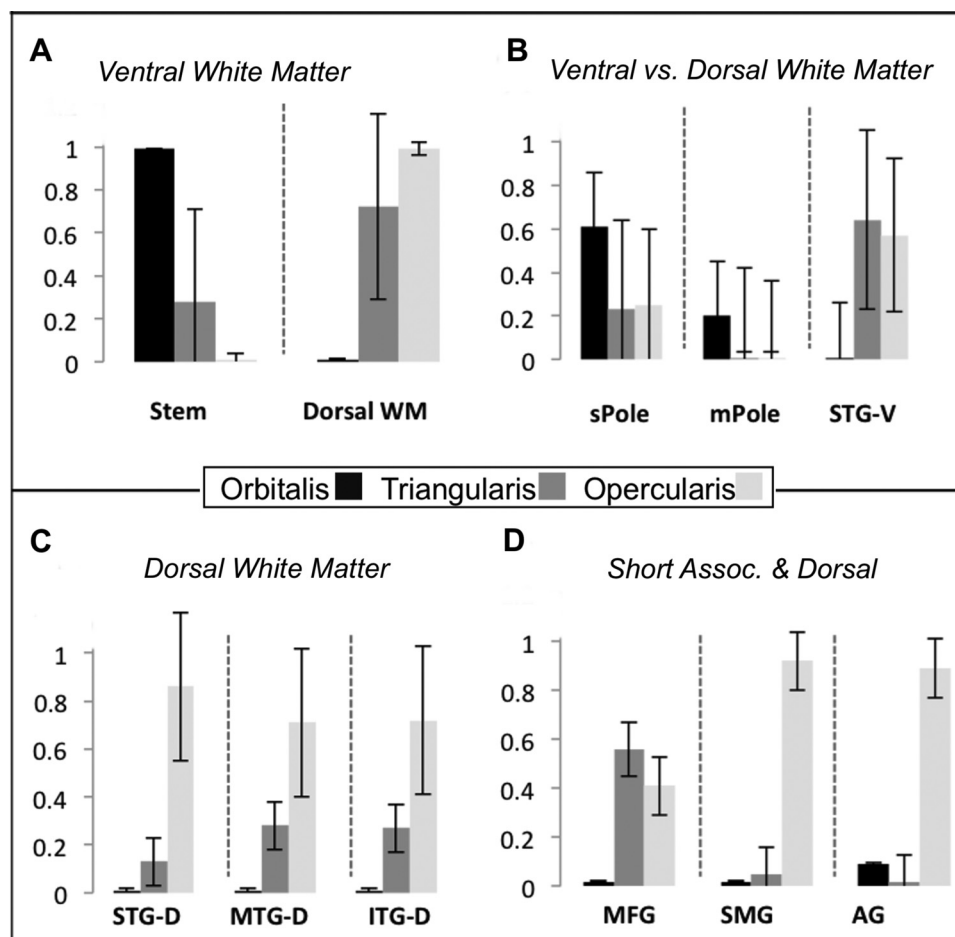


Fig. 3. Anatomical connectivity of macro-anatomical VLPFC subregions via the ventral and dorsal path white matter seeds. *A*: mean % of fiber streamlines from each macro-anatomical division by ventral or dorsal anatomical pathway. *B*: mean % of fiber streamlines from each macro-anatomical division anatomically connected to temporal lobe targets by the ventral white matter. *C*: mean % of fiber streamlines from each macro-anatomical division anatomically connected to temporal lobe targets by the dorsal white matter. *D*: mean % of fiber streamlines from each macro-anatomical division anatomically connected with targets in the frontal and parietal cortices. Error bars depict SD.

lobe. For brevity, we only report comparisons that were reliable first in omnibus Friedman's nonparametric ANOVA and then in pairwise contrasts, corrected for multiple comparisons (all $P < 0.05$).

The ventral white matter primarily connected VLPFC to rostral temporal cortex, with all three VLPFC subregions connecting to superior temporal pole (sPole) by this route. Furthermore, orbitalis had a greater number of connections to sPole and middle temporal pole (mPole) than the other VLPFC subregions (Fig. 3*B*).

The dorsal white matter primarily connected VLPFC with dorsal and lateral temporal cortex, caudal to the temporal pole. The densities of fiber streamlines to STG, middle temporal gyrus (MTG), and inferior temporal gyrus (ITG) all demonstrated the same pattern (Fig. 3*C*): density to temporal targets increased in the caudal direction along the rostrocaudal axis of IFG (opercularis > triangularis > orbitalis; all $t > 2.6$, $P < 0.01$).

In summary, fiber tracks connecting VLPFC to temporal cortex via the white matter of the temporal stem preferentially targeted superior and rostral temporal cortex connections (i.e., sPole and mPole) and originated primarily from rostral VLPFC (Fig. 3*B*). By contrast, caudal regions of VLPFC exhibited a higher density of connection via SLF and the arcuate (i.e., opercularis > triangularis > orbitalis) with caudal and ventral temporal cortex than rostral regions (Fig. 3*C*).

VLPFC connections with parietal cortex. We next investigated connections between VLPFC and parietal subregions. As

with the preceding analyses, we only report effects that were statistically significant both in omnibus comparison and in contrasts corrected for multiple comparisons (all $P < 0.05$). No tracts with parietal cortex were discovered via the temporal stem seed. Thus here we focus only on tracts reconstructed through the dorsal white matter seed (Fig. 3*D*).

All three VLPFC subregions were more densely connected with supramarginal gyrus (SMG) than angular gyrus (AG), although this effect was only trending in pars triangularis ($Z = 2.04$, $P = 0.12$). Although we resolved more connections between VLPFC and SMG than AG, we note that this difference may reflect differences in the inherent difficulty of resolving tracts to AG given the confluence of crossing fiber tracts proximal to AG. Between-VLPFC subregion comparisons indicated that the pars opercularis subregion was connected most densely with both parietal subregions (AG, SMG) relative to the other VLPFC subregions. Triangularis was marginally more connected to SMG than orbitalis ($Z > 2.30$, $P = 0.06$).

Thus fiber tracking indicated that VLPFC projections target the parietal cortex via the dorsal white matter rather than the temporal stem. Overall, anatomical connectivity of VLPFC with the parietal cortex increases in the caudal direction, peaking in pars opercularis (Fig. 3*D*). All subregions exhibited the greatest connectivity with SMG relative to AG.

VLPFC connections with dorsolateral frontal cortex. We next examined connectivity of VLPFC subregions to MFG through the ascending white frontal matter, presumably reflect-

ing the short U fibers (Fig. 3D). A one-way Friedman's nonparametric ANOVA indicated that VLPFC regions differed in their overall connectivity with MFG [$\chi^2(2) = 26.00, P < 0.0001$]. Follow-up paired tests showed that triangularis-MFG connectivity exceeded that of orbitalis ($Z = 3.82, P < 0.0005$). Opercularis also exhibited greater connectivity to MFG than orbitalis ($Z = 3.78, P < 0.0005$). Opercularis and triangularis fiber tracks, however, were equally represented ($Z = 0.76, P > 0.40$). Thus all regions of VLPFC were connected with MFG, but triangularis and opercularis connection density exceeded that of orbitalis.

Summary of connectivity distribution analysis. In summary, the anatomical connectivity of orbitalis is biased toward the anterior temporal lobe via the ventral white matter, while triangularis is connected with SMG via the dorsal white matter, the temporal lobes via both the dorsal and ventral white matter, and connected to frontal cortex by the short U fibers. The pars opercularis is connected anatomically with the temporal lobes and parietal cortex primarily via the dorsal white matter and is also connected to frontal cortex by U fibers. Thus, overall, connections via the ventral vs. dorsal white matter distributions followed an approximate rostral-to-caudal gradient. However, in what follows, our analysis suggests that rather than being rostro-caudal, per se, this pattern reflects at least two dorsal and

ventral cortical zones that run roughly parallel to each other within the VLPFC.

Topographic Microorganization Analysis

Next, we conducted topographic microorganization analysis to investigate whether the underlying white matter anatomy of left VLPFC yields finer anatomical divisions based on extrinsic connectivity with dorsal and ventral path targets, as defined in the preceding section. Only fiber track pairs where seeding produced streamlines in at least half of participants (median > 0) were included in the analysis.

Segmentation of pars orbitalis. The anatomical profile of the pars orbitalis region of VLPFC is dominated by ventral path projections with anterior temporal cortex, particularly within temporopolar regions. The only other region having observed anatomical connectivity with orbitalis was MFG in the frontal cortex (Fig. 4, A–C).

Figure 4, D and E, plot the distribution of end points to temporal lobe and MFG within orbitalis, collapsing over the axial (Fig. 4D) and sagittal (Fig. 4E) planes. Notably, ventral white matter connections were distributed ventral and caudally, whereas the dorsal white matter and U-fiber connections to frontal cortex were dorsal. A reliable region \times dimension interaction [Wilks's lambda = 0.004, $F(8,11) = 368.13, P <$

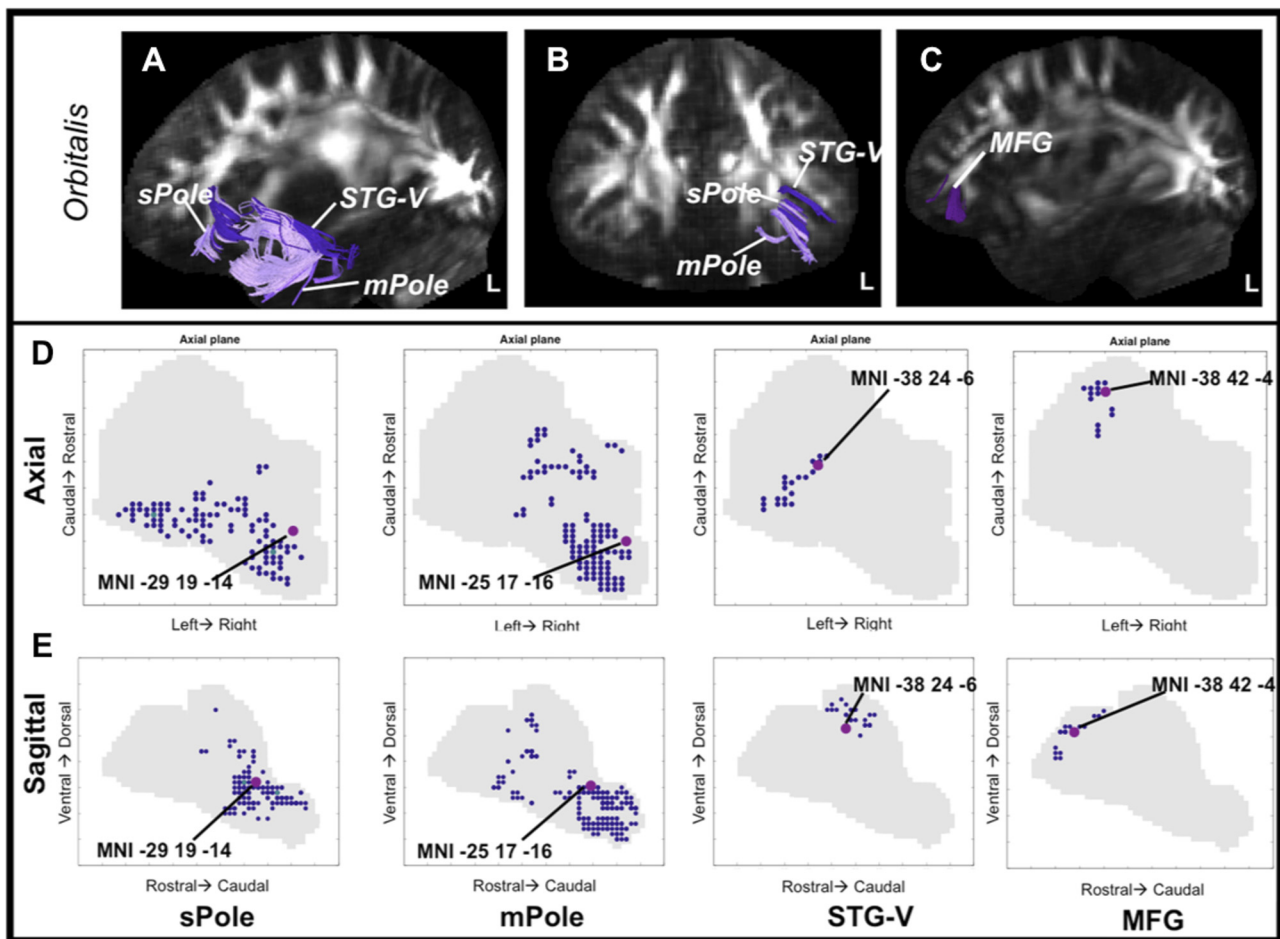


Fig. 4. Extrinsic anatomical connectivity of the pars orbitalis. A and B: example of fiber streamlines connecting orbitalis to sPole, mPole, and STG via the ventral white matter in a representative subject. C: example of fiber streamlines from orbitalis to MFG via the short association fibers. D and E: spatial distribution of end points in VLPFC by target region. Large dots indicate the position of the average center of mass, the location where projection end points are most dense, in MNI coordinates. D: streamline end points in the axial plane. E: end points in the sagittal plane.

0.0001] indicated that sPole, mPole, STG, and MFG end-point centers of mass are separable from one another. To ask whether the ventral white matter end points (sPole, mPole, and STG-V) terminate in a region of pars orbitalis separate from the MFG end points, the ventral end points were averaged and compared with those from MFG. The averaged ventral path center of mass was ventral, caudal, and medial to that of MFG (all $Z > 3.50$, $P < 0.001$), indicating that temporal stem and short association streamlines terminate in different orbitalis subregions.

Segmentation of pars triangularis. The pars triangularis is connected extensively with frontal and temporal cortices through both the ventral and dorsal white matter. Temporal fiber streamlines to triangularis are depicted in Fig. 5, *A* and *B*, and frontal and parietal in Fig. 7, *A* and *B*. A reliable region \times dimension interaction indicated that the centers of mass associated with dorsal and ventral white matter and frontal end points differed in their spatial distribution [Wilks's lambda = 0.008, $F(12,7) = 68.21$, $P < 0.0001$]. The averaged dorsal

white matter end-point center of mass was separable from MFG end points in triangularis along all three spatial dimensions (all $Z > 3.06$, $P < 0.05$), suggesting that although the association fiber zone is located in dorsal triangularis like the dorsal white matter projection zone it constitutes a distinct population. Additionally, testing the dorsal path center of mass against the ventral white matter STG center indicated that ventral path end points are rostral, medial, and ventral to dorsal path end points (all $Z > 2.58$, $P < 0.01$). See Fig. 5, *C* and *D*, for graphic representation of the distribution of temporal projection end points in triangularis, and Fig. 7, *E* and *F*, left (plotted in green) for frontal and parietal end-point distributions.

Segmentation of pars opercularis. Of the three VLPFC subregions, the pars opercularis end points came from a broad set of temporal, frontal, and parietal areas. Figure 6, *A* and *B*, plots projections from opercularis to temporal cortex; the distribution of temporal end points is plotted in Fig. 6, *C* and *D*. Figure 7, *C* and *D*, plot the projections to the frontal and

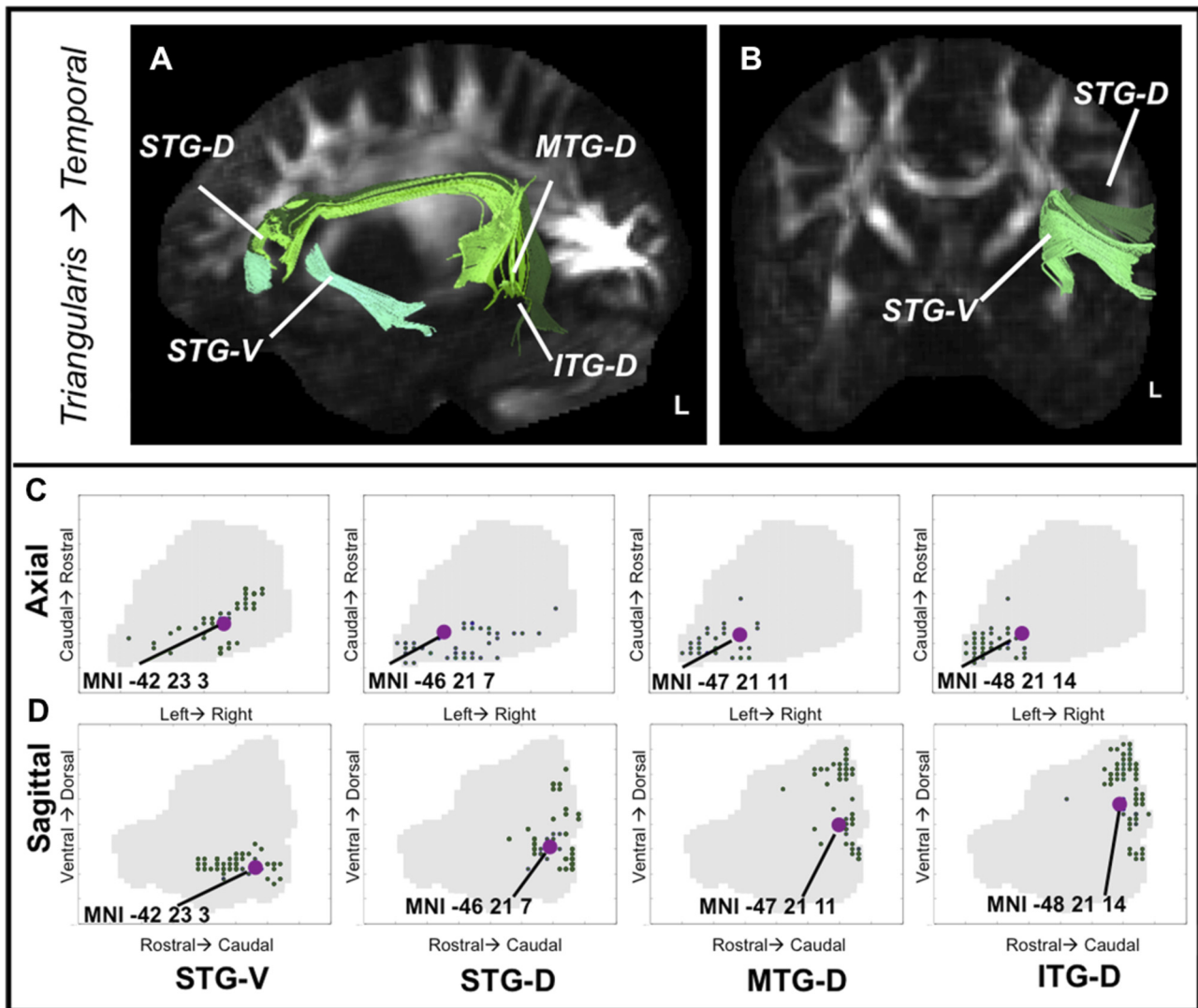


Fig. 5. Extrinsic anatomical connectivity of the pars triangularis to temporal cortex. *A* and *B*: examples of fiber streamlines connecting triangularis to STG, MTG, and ITG in a representative subject. Suffix “-V” or “-D” refers to the seed used to generate fiber streamlines (ventral or dorsal white matter). *C* and *D*: spatial distribution of projection end points in VLPFC by target region. Large dots indicate the position of the average center of mass, the location where projection end points are most dense, in MNI coordinates. *C*: end points in the axial plane. *D*: projection end points plotted in the sagittal plane.

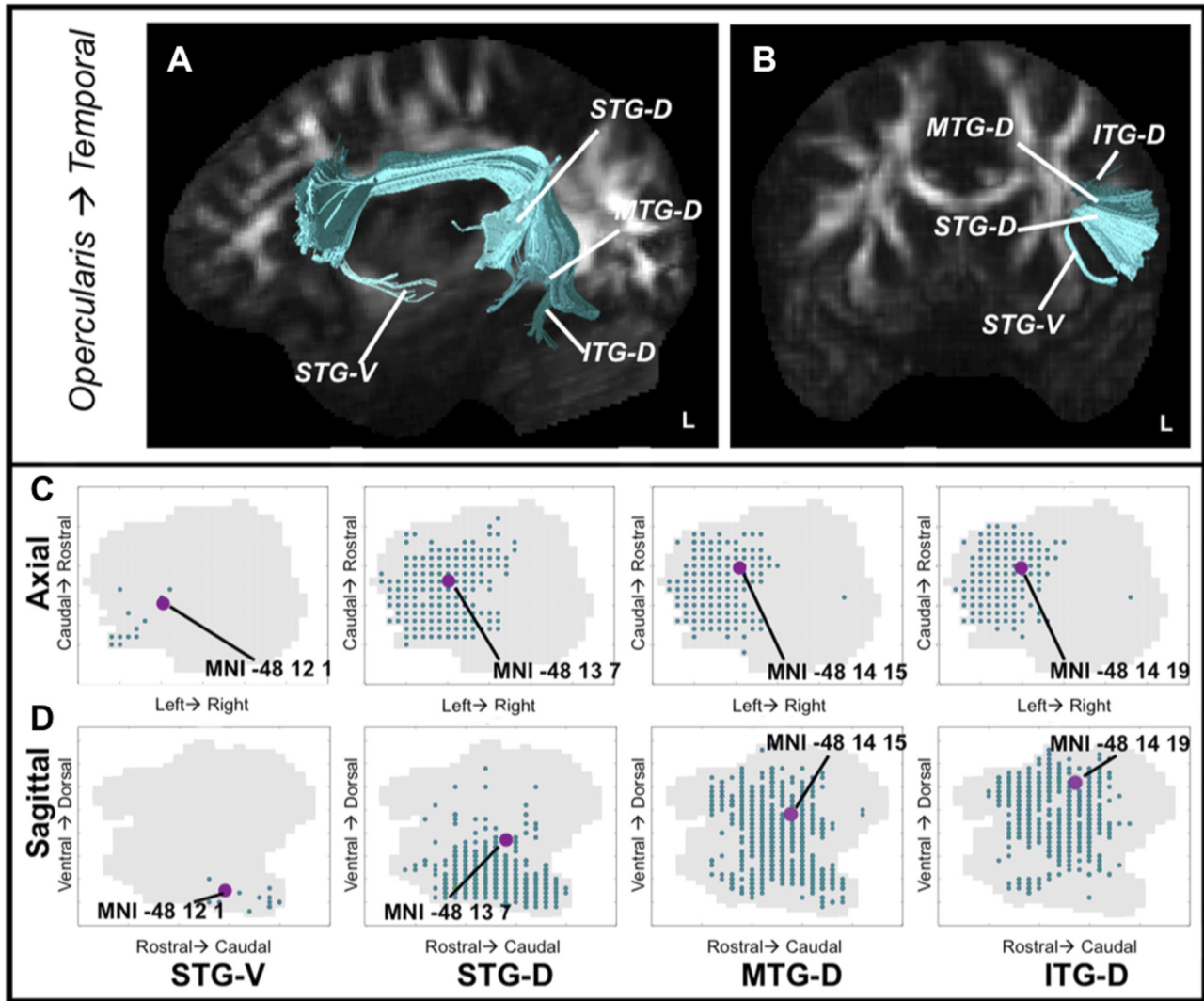


Fig. 6. Extrinsic connectivity of the pars opercularis to temporal cortex. *A* and *B*: examples of fiber streamlines connecting opercularis to STG, MTG, and ITG in a representative subject. Suffix “-V” or “-D” refers to the seed used to generate fiber streamlines (ventral or dorsal white matter). *C* and *D*: spatial distribution of projection end points in VLPFC by target region. Large dots indicate the position of the average center of mass, the location where projection end points are most dense, in MNI coordinates. *C*: end points in the axial plane. *D*: projection end point locations in the sagittal plane.

parietal lobes within opercularis, collapsing across the axial and sagittal planes.

The pars opercularis is small relative to pars orbitalis and triangularis, yet centers of mass still divided into distinct zones. A statistically significant region \times dimension interaction demonstrated that end-point populations were separable [Wilks's lambda = 0.094, $F(6,13) = 21.00$, $P < 0.0001$]. Follow-up comparisons indicated that STG end points resulting from the ventral white matter seeding were ventral, caudal, and lateral to the average of the dorsal path (STG, MTG, ITG, SMG, and AG) centers of mass (all $Z > 3.10$, $P < 0.05$). Pars opercularis end points from MFG were also distinct from dorsal white matter end points and were situated within the rostral and dorsomedial aspect of opercularis (all $Z > 3.8$, $P < 0.001$). MFG end points were dorsal to ventral white matter (STG) end points ($Z = 3.8$, $P < 0.001$).

Summary of microorganization analysis. Taken together, our analysis of VLPFC projections suggests that in general the rostroventral aspect of VLPFC is extrinsically connected to other cortical regions via the ventral white matter of the

temporal stem, while dorsocaudal VLPFC projections mainly follow the trajectory of the SLF and arcuate fasciculus. Across IFG, the ventral areas contained projections from temporal stem STG fiber streamlines and in the case of pars orbitalis end points of temporopolar cortex streamlines. Dorsal and caudal VLPFC projections, however, originated from caudal and inferior regions of temporal cortex, as well as parietal cortex in the case of pars opercularis. See Table 3 for the locations of end points in IFG.

MFG end points from the short association streamlines were clustered in the dorsal VLPFC across subregions but were more numerous from caudal IFG. These MFG projection zones were always dorsal to end points generated by temporal stem seeding, suggesting that connections to DLPFC in general originate from dorsal rather than ventral VLPFC. This organizational principle is further emphasized by the relative sparseness of orbitalis-MFG fiber streamlines.

Fiber streamlines to parietal cortex are a feature of caudal not rostral IFG. End points from fiber streamlines connecting IFG to SMG were observed in ventrocaudal triangularis and

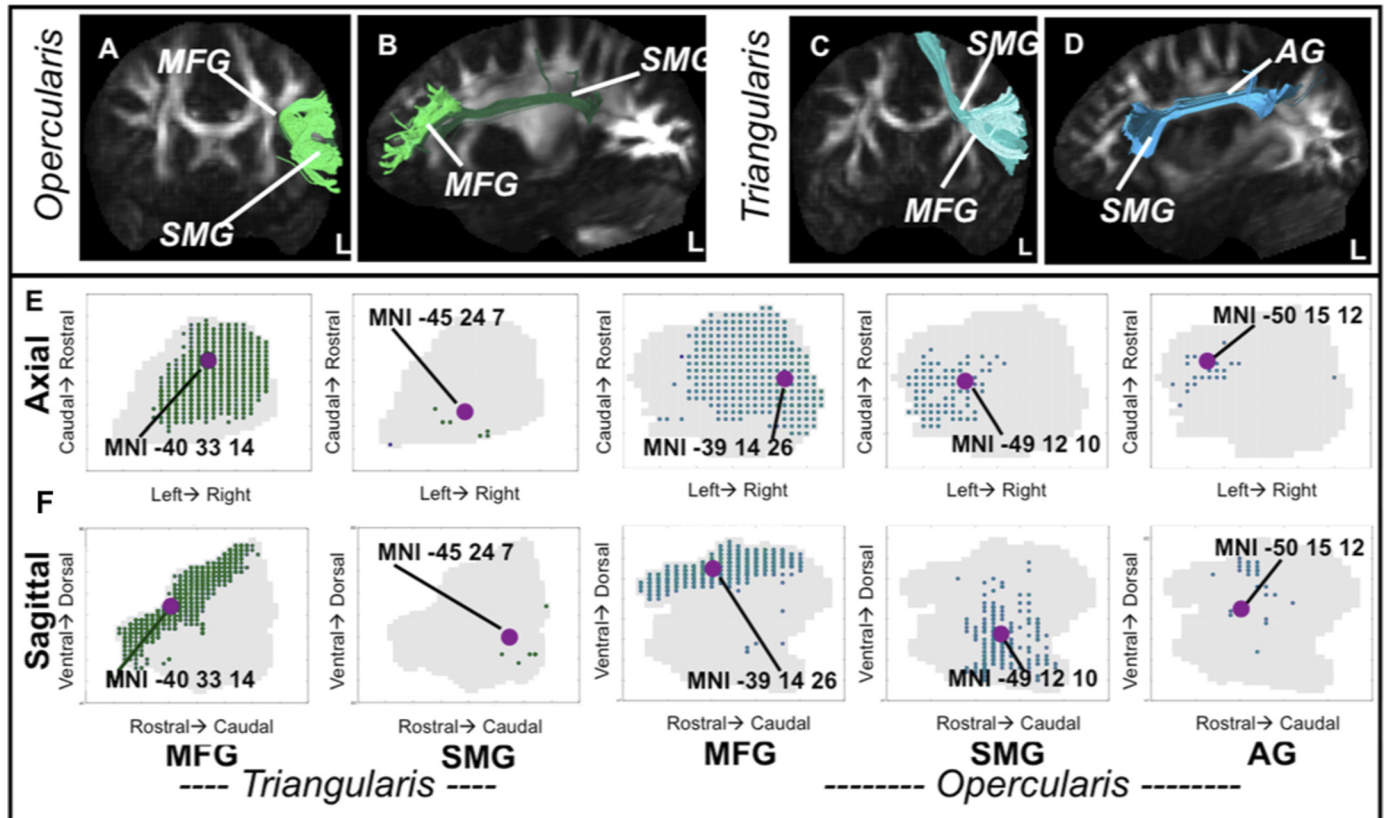


Fig. 7. Extrinsic connectivity of pars triangularis and opercularis to MFG and parietal cortex. *A* and *B*: examples of fiber streamlines connecting triangularis to MFG and SMG in a representative subject. *C* and *D*: examples of fiber streamlines connecting opercularis to MFG, SMG, and AG. *E* and *F*: spatial distribution of end points in VLPFC by target region. Large dots indicate the position of the average center of mass, the location where projection end points are most dense, in MNI coordinates. *E*: projection end points in the axial plane. *F*: end points in the sagittal plane.

ventral opercularis. End points from AG fibers in opercularis were dorsal to SMG end points; other IFG subregions did not reliably produce tracks to AG (both medians = 0).

Thus, overall, it appears that rather than lining up in terms of classical macroanatomical distinctions, such as between orbitalis and triangularis, VLPFC cortical targets of the ventral and dorsal pathways may run in parallel to each other along a dorsal-ventral organization in the IFG. We return to this point in DISCUSSION.

Functional Connectivity

Finally, we sought to establish that the projection zones identified in our white matter segmentation analyses correlate with regions within the broader distinct functional connectivity networks defined by Barredo et al. (2015). To examine functional connectivity networks associated with our segmentation zones, we constructed sphere ROIs using the coordinates from end-point centers of mass produced by our VLPFC fiber streamline tracking. These ROIs were then used as seed regions for functional connectivity analysis in the same group of participants.

Ventral pathway functional networks. The functional connectivity networks generated from seeds corresponding to temporal stem centers of mass produced networks consistent with parts of the “ventral pathway” implicated in controlled retrieval from memory by our prior functional work (Barredo et al. 2015). For a full report of reliable clusters associated with each of the ventral pathway seeds, see Table 4.

The orbitalis-sPole network (Fig. 8*E*) approximated features of the frontotemporal retrieval network (Fig. 8*D*) as did the orbitalis-mPole network, though overall connectivity was reduced in the orbitalis-mPole network (Fig. 8*F*). The orbitalis-sPole seed was correlated with large bilateral clusters in orbitalis that extended into the temporal pole (Fig. 8*E*). Reliable functional coupling with frontal pole, left AG, bilateral parahippocampal gyrus, and right hippocampus was also observed

Table 3. VLPFC end-point center of mass locations

ROI Pair	MNI Coordinates		
	x_{VLPFC}	y_{VLPFC}	z_{VLPFC}
orb-sPole	-29	19	-14
orb-mPole	-25	17	-16
orb-stgV	-38	24	-6
orb-mfg	-38	42	-4
tri-stgV	-42	23	3
tri-stgD	-46	21	7
tri-mtgD	-47	21	11
tri-itgD	-48	21	14
tri-mfg	-40	33	14
tri-smg	-45	24	7
op-stgV	-48	12	1
op-stgD	-48	13	7
op-mtgD	-49	14	15
op-itgD	-49	4	19
op-mfg	-39	14	26
op-smg	-49	12	10
op-ang	-50	15	12

Table 4. Ventral pathway functional connectivity networks

Seed	Peak Location	x	y	z	t-Value	
Orb.-sPole	L. Orb./Insula	-27	15	-15	19.1	
	R. Frontal pole	9	69	15	8.3	
	R. Orb.	51	21	-6	8.8	
	R. PHG	21	-48	-9	7.5	
	L. Mid-Occ.	-36	-93	15	6.8	
	L. Angular	-48	-63	39	6.7	
	R. Mid-Occ.	33	-90	18	8.7	
	L. Precuneus	-3	-78	42	9.6	
	L. Mid-cingulate	-3	15	45	6.8	
	R. SFG	12	24	63	7.1	
	R. mPole	48	6	-36	5.2	
	R. Precuneus	18	-87	45	5.7	
	R. STG	57	-60	27	5.6	
	R. HPC	33	-24	-12	5.8	
	R. Insula	42	-18	15	5.5	
	L. PHG	-27	-24	-21	5.3	
	R. Postcentral	15	-51	72	5.0	
	L. Precuneus	-24	-90	48	4.9	
	L. Postcentral	-27	-42	63	5.4	
	Orb.-mPole	L. Orbitalis	-27	21	-15	10.7
L. Frontal pole		-18	63	30	7.9	
R. Orbitalis		24	18	-18	6.5	
L. Angular		-48	-57	36	8.1	
L. Precuneus		-6	-78	36	7.1	
R. mPole		36	18	-42	6.6	
R. ITG		57	-9	-33	6	
L. P. Cingulate		-3	-51	15	5.2	
L. TPJ		-54	-36	24	5.5	
L. MTG		-69	-27	-3	6.4	
SFG		0	33	63	6.2	
L. Mid-Occ.		-48	-87	3	4.8	
R. Lingual		27	-78	-9	5	
R. Mid-Occ		9	-95	12	5.3	
L. Precentral		-57	6	15	5.6	
L. SFG		-18	24	57	5.9	
L. MTG		-45	-9	-18	4.8	
R. SFG		21	63	27	5.1	
Orb.-STGv		L. Med. FC	-3	42	39	10.9
		L. Orb.	-42	24	-9	27.1
	R. Orb.	45	21	-6	10.1	
	L. Cuneus	-9	-72	-6	7.4	
	L. Temporal pole	-51	-6	-42	6	
	L. Mid-Occ.	-42	-84	12	6	
	L. MFG	-39	12	48	5.9	
	R. STG	54	-15	9	5.8	
	R. TPJ	48	-36	24	7	
	R. PHG	27	-57	-6	6.9	
	L. MTG	-60	-69	0	5.2	
	L. SFG	-24	3	75	6.9	
	R. Precuneus	15	-48	63	5.1	
	R. Fusiform	48	-54	-21	5.1	
	R. STG	48	-21	0	5.8	
L. MFG	-18	57	-3	5		
Tri.-STGv	L. Triangularis	-45	24	3	23.3	
	L. TPJ	-54	-60	18	8.8	
	R. Orbitalis	54	24	0	7.8	
	L. Med. FC	0	15	51	7.5	
	L. Cingulate	-6	3	51	6.4	
	L. MFG	-27	54	24	6.8	
	R. Cuneus	12	-99	3	6.1	
	R. Fusiform	42	-48	-18	7.9	
	R. STG	54	-42	9	6.4	
	R. Insula	48	12	0	11.8	
Op.-STGv	L. Insula	-48	12	0	6.9	
	L. Cingulate	-6	14	42	6.8	
	L. IPL/IPS	-28	-46	56	6.2	
	L. MTG	-58	-64	14	5.9	
	R. Precuneus	14	-40	48	5.7	
	L. Precentral	-46	-16	48	6.8	

(Fig. 8E). Similarly, the orbitalis-mPole seed was also correlated with bilateral orbitalis, left temporal pole, frontal pole, and AG (Fig. 8F).

The connectivity networks of the orbitalis, triangularis, and opercularis seeds from the ventral white matter STG streamlines all overlapped with IFG/insula and posterior regions of the frontotemporal retrieval network (Fig. 8, A–C). Prominent clusters in the orbitalis- and triangularis-STGv networks had peaks proximal to the seed (Fig. 8, A and B), while in the opercularis-STGv network the peak voxel was located posterior to opercularis in STG (Fig. 8C). This large STG peak cluster in the opercularis network extended from mid-IFG to left temporo-parietal junction (TPJ) (Fig. 8F). Large left TPJ clusters were also observed in the orbitalis and triangularis networks (Fig. 8, D and E). Large clusters extending from IFG to posterior temporal cortex were also present in all three IFG-STGv functional networks in the right hemisphere. For full details see Table 4.

In conclusion, the functional connectivity networks of the VLPFC ventral white matter seeds exhibit functional connectivity consistent with the ventral frontotemporal network involved in episodic retrieval (Barredo et al. 2015; Fig. 8D). Seed networks associated with orbitalis-sPole center of mass recapitulated the temporopolar portion of the ventral frontotemporal network (Fig. 8E), while the connectivity networks of the STG ventral pathway centers of mass exhibited more extensive connectivity with parts of the ventral frontotemporal network in posterior temporal cortex/TPJ (Fig. 8, A–C).

MFG-short association functional networks. The functional network associated with postretrieval control identified in Barredo et al. (2015) encompasses the pars triangularis, MFG, and parietal cortex near the IPS. Given the high degree of connectivity of both dorsal triangularis and opercularis with MFG, we anticipated that functional connectivity networks associated with seeds from these centers of mass would be distributed in a similar manner as the previously defined dorsal postretrieval network (Fig. 9A). Indeed, the networks generated from the IFG-MFG seeds recapitulate the MFG connectivity observed in the postretrieval functional network (Fig. 9). There were some connectivity differences within this overall dorsal frontal network. Perhaps most notable is the connectivity of pars orbitalis with separate portions of MFG positioned more rostral and dorso-caudal to the broader swath of middle MFG that connected with triangularis and opercularis. Whether these separate patterns reflect functional differences remains to be determined, though the pattern of connectivity along MFG between orbitalis vs. triangularis/opercularis appears to map roughly to frontopolar vs. mid-lateral frontal subnetworks within the broader fronto-parietal control system that have been observed previously (Yeo et al. 2011). The triangularis- and opercularis-MFG seeds also exhibited connectivity with IPS, another defining characteristic of the postretrieval network (Fig. 9, A, C, and D). The full list of reliable peaks from the functional connectivity networks of the short association fiber centers of mass can be found in Table 5.

Dorsal white matter functional networks. Next we examined the functional connectivity of VLPFC seeds that connect to temporal (Fig. 8, G–L) and parietal cortex via the dorsal white matter (Fig. 10). Streamlines connecting orbitalis to either temporal or parietal target regions via the dorsal pathway were not reliably observed, and thus no centers of mass were

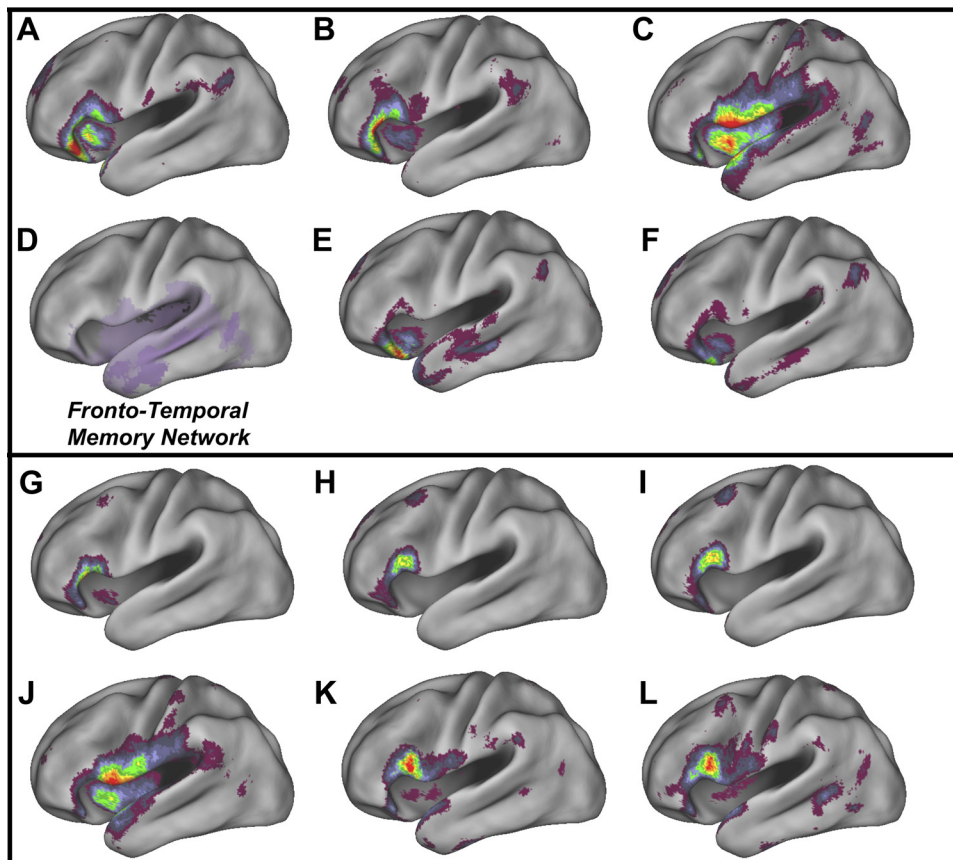


Fig. 8. Relationship of the functional connectivity networks of the ventral and dorsal white matter seeds to the fronto-temporal memory retrieval network. The center of mass networks from the VLPFC ventral white matter seeds exhibit functional connectivity consistent with the ventral fronto-temporal network involved in episodic retrieval (Barredo et al. 2015). Panels display the left sagittal view of the locations of statistically reliable functional connectivity clusters associated with the following IFG end-point center of mass seeds: orbitalis-STGv (A); triangularis-STGv (B); opercularis-STGv (C); the fronto-temporal memory retrieval network of Barredo et al. (2015) (D); orbitalis-sPole (E); orbitalis-mPole (F); triangularis-STGd (G); triangularis-MTGd (H); triangularis-ITGd (I); opercularis-STGd (J); opercularis-MTGd (K); opercularis-ITGd (L). Minimum thresholds are set at $P < 0.001$ uncorrected (violet), maximum value at $t \geq 10.0$ (red).

available from dorsal pathway seeds for this analysis. On the basis of our tractography results, we predicted a priori that dorsal white matter seeds would exhibit greater connectivity with caudal temporal cortex regions than ventral white matter seeds. The data were consistent with this prediction in pars opercularis: functional connectivity networks associated with each center of mass were characterized by a widespread cluster emanating from the seed location that followed the trajectory of the SLF and arcuate fasciculus to caudal temporal cortex (Fig. 8, J–L). The caudal temporal and parietal cortices near TPJ were common lateral cortical targets of the opercularis dorsal white matter seeds. Thus functional networks associated with these opercularis seeds shared more common features with the ventral (Fig. 8D) rather than dorsal functional network (Fig. 9A) described by Barredo et al. (2015). However, the pars triangularis dorsal white matter networks (Fig. 8, G–I)—with the exception of the triangularis-SMG network (Fig. 10A)—were comprised mainly of anterior rather than posterior ventral retrieval pathway regions (Fig. 8D).

In summary, overall the functional networks associated with dorsal pathway seeds were comparable to the ventral retrieval network of Barredo et al. 2015 (Fig. 8D) rather than the postretrieval control network (Fig. 9A) or other resting-state functional connectivity networks associated with cognitive control networks (Power and Petersen 2013; Vincent et al. 2008; Yeo et al. 2011). Furthermore, in agreement with our tractography results, a rostral-to-caudal shift in functional connectivity was observed within these dorsal pathway seeds such that greater connectivity with parietal and posterior temporal cortex was exhibited by caudal IFG. See Table 6 for a full

summary of cluster peaks associated with the dorsal pathway seeds.

DISCUSSION

Here we provide evidence for a functional organization of left VLPFC based on the topology of its extrinsic anatomical

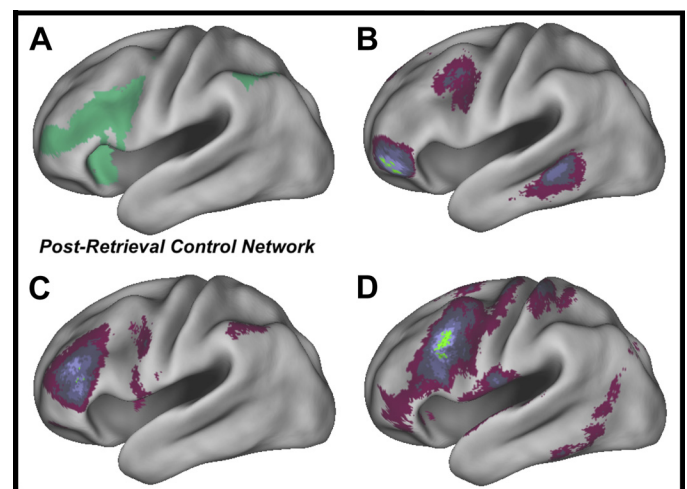


Fig. 9. Relationship of the functional connectivity networks of the IFG-MFG seeds connected anatomically by the short association U fibers and the postretrieval control network. A: the functional connectivity network implicated in postretrieval control by Barredo et al. (2015). B–D: left sagittal views of the locations of statistically reliable functional connectivity clusters associated with the following IFG end-point center of mass seeds: orbitalis-MFG (B); triangularis-MFG (C); opercularis-MFG (D). Minimum thresholds are set at $P < 0.001$ uncorrected (violet), maximum value at $t \geq 10.0$ (red).

Table 5. *MFG-short association fiber functional connectivity networks*

Center of Mass	Peak Location	x	y	z	t-Value
Orb.-MFG	L. MTG	-66	-33	-9	7.5
	L. Orb.	-48	45	-15	9.8
	L. MFG	-51	18	33	5.9
	L. Med. FC	-9	33	45	6.2
	L. SFG	-15	48	39	7
Tri.-MFG	L. MFG	-39	33	18	11.4
	L. AG	-57	-51	48	5
	L. MFG	-33	45	-9	5.7
Op.-MFG	L. MFG	-39	15	30	16.2
	L. SPL	-21	-69	60	5.3
	SFG	0	-9	72	6.4
	L. Cingulate	-9	21	42	6.1
	R. Opercularis	54	21	24	5.6
	R. Paracentral	9	-36	69	5.3
	L. MFG	-51	48	-9	4.8
	L. Postcentral	-57	-6	18	5.2
	L. MTG	-54	-42	-18	5.7
	R. STG	66	-33	18	5.2
	R. MTG	51	-75	21	5.1
	L. Lingual	-15	-54	-3	5.2
	L. MTG	-45	-63	12	5.3
	R. Postcentral	51	-30	66	6.6
	R. SFG	9	12	63	6.3
	R. Orbitalis	27	30	-12	5.1
	L. STG	-57	6	-3	5.2
	R. SPL	12	-84	60	4.9
	R. SPL	33	-66	63	4.9
	R. Precentral	36	-30	72	4.9

connections and functional connectivity to other brain regions. Our findings complement models proposing that lateral PFC is comprised of dorsal and ventral functional subregions corresponding roughly to DLPFC and VLPFC (Blumenfeld et al. 2012; O'Reilly 2010; Petrides 2005), as well as recent connectivity-based parcellations of the VLPFC (Neubert et al. 2014). Our use of high-angular-resolution, deterministic tractography allowed us to investigate specific white matter pathways—identified in prior functional work as crucial for fronto-temporal interactions during memory retrieval—and to observe in fine detail the end points of fiber streamlines within IFG even in regions with a high degree of tract interdigitation. Streamline distribution and segmentation results indicate that the dorsal aspect of IFG exhibits a pattern of anatomical connectivity that is distinct from that of ventral IFG. This dorsal/ventral pattern of organization holds across the conventional macroanatomical subdivisions of IFG. Furthermore, similarities between the topography of functional networks associated with the dorsal IFG and functional connectivity patterns associated with DLPFC support the assertion that dorsal VLPFC should be functionally grouped with DLPFC.

Additionally, the results of the segmentation analysis indicated that within ventral IFG a more refined organization of extrinsic anatomical connections exists. Anatomical connectivity within ventral IFG was biased such that streamlines from ventral and rostral areas tended to project through the ventral white matter pathway whereas streamlines from dorsal and caudal areas tended to project through the dorsal white matter pathway. We now examine these anatomically constrained ventral and dorsal left IFG networks in greater detail and consider their connection with cognitive control processes involved in memory.

Consistent with neuroanatomical tracer studies in nonhuman primates, our tractography results indicated that the number of ventral IFG streamlines projecting through the ventral white matter pathway decreases along the caudal axis, while streamlines projecting through the dorsal pathway increase. Thus the two pathways here are similar to the ventral and dorsal streams described in the macaque by Petrides and Pandya (2009). In macaque IFG, the orbitalis and triangularis homologs project to rostral temporal cortex and intermediate STG through fibers of the uncinate fasciculus and the EFCS (Barbas 1988; Petrides and Pandya 2002, 2009). Although both subregions of the macaque triangularis homolog project through this ventral white matter pathway, the density of this projection decreases from 45A to 45B (Gerbella et al. 2010; Petrides and Pandya 2009). Relatively few projections from neighboring macaque 44 are part of this ventral fronto-temporal stream (Petrides and Pandya 2009). Our findings are also consistent with reports of inferior parietal lobule and intermediate-to-caudal STG connectivity via a dorsal stream of fibers that is more prominent in mid- to caudal IFG in the macaque (Petrides and Pandya 2009).

The streamline trajectories associated with the ventral and dorsal pathways here resembled distinct fiber bundles described in earlier human tractography studies. The trajectories of ventral pathway streamlines with end points in the ventral-most extent of IFG terminating in the temporal pole were similar to earlier characterizations of the uncinate fasciculus (Crosson et al. 2005; Thibaut de Schotten et al. 2012), while the trajectories of streamlines from more dorsal ventral pathway centers of mass resembled those of the EFCS (Frey et al. 2008; Makris and Pandya 2009). The route of dorsal pathway streamlines was similar to that of the arcuate fasciculus (Catani et al. 2005; Thibaut de Schotten et al. 2012) and the SLF (Crosson et al. 2005; Frey et al. 2008).

This finer-grained segmentation of the ventral pathway is relevant to proposed functional distinctions between VLPFC subregions that contribute to the cognitive control of memory. It has been suggested that a functional aVLPFC subregion (approximating pars orbitalis) contributes to controlled mem-

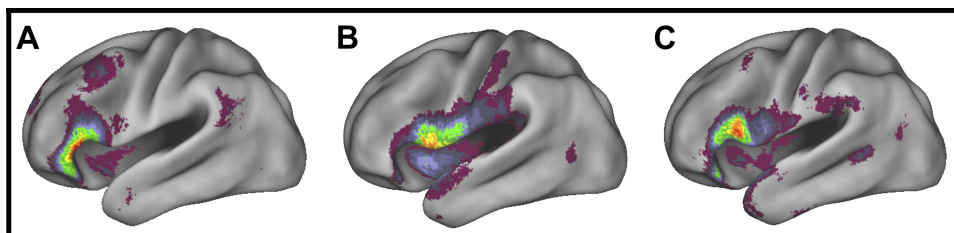


Fig. 10. Functional connectivity networks of the dorsal white matter pathway IFG-parietal cortex center of mass seeds. Panels display locations of statistically reliable functional connectivity clusters in the left hemisphere associated with the following IFG end-point center of mass seeds: triangularis-SMG (A); opercularis-SMG (B); opercularis-AG (C). Minimum thresholds are set at $P < 0.001$ uncorrected (violet), maximum value at $t \geq 10.0$ (red).

Table 6. *Dorsal white matter functional connectivity networks*

Center of Mass	Peak Location	x	y	z	t-Value
Tri-STG	L. Triangularis	-48	21	6	20
	R. Triangularis	54	24	0	6.8
	L. MFG	-3	45	42	6.1
	L. TPJ	-54	-60	15	5.2
	L. MFG	-39	6	51	5.6
	L. Postcentral	-27	-45	66	6.6
	L. SFG	-18	54	24	5.3
	R. MFG	39	12	36	5.8
	L. Insula	-36	-6	-12	5
	L. MFG	-54	18	30	4.9
Tri-MTG	L. Triangularis	-51	21	12	14
	MFG	0	39	48	7.3
	L. TPJ	-63	-57	24	6.9
	R. Orbitalis	51	27	-12	8.3
	L. MFG	-45	21	45	7
	R. ITG	33	0	-45	6.9
	L. Postcentral	-21	-48	66	5.5
	R. STG	57	-36	12	6
	L. Triangularis	-51	21	15	16.6
	R. SFG	6	27	60	8
Tri-ITG	L. TPJ	-51	-60	24	6.5
	R. Orbitalis	48	27	-12	9.7
	L. Uncus	-24	-9	-33	6.6
	L. SFG	-18	45	36	6.1
	R. Triangularis	54	24	24	6.3
	R. Insula	51	-39	18	5.1
	R. Uncus	30	3	-48	6.1
	L. Precentral	-66	-12	30	5.1
	L. Postcentral	-21	-48	69	6
	L. MTG	-63	-63	9	4.8
Tri-SMG	L. Orbitalis	-42	24	6	21.8
	L. TPJ	-54	-57	15	5.5
	R. Orbitalis	51	27	0	6.6
	L. SFG	-18	54	45	5.5
	L. Frontal pole	-24	57	24	6.5
	L. Postcentral	-27	-42	72	6.5
	L. IPL	-48	-51	60	5.4
	L. PHG	-42	-30	-30	5.8
	L. SFG	-6	-12	75	6.7
	L. ITG	-51	-54	-18	5.3
Op-STGd	L. SFG	-21	-9	72	4.8
	R. MTG	42	3	-39	5.6
	L. MTG	-54	9	-24	4.8
	L. Insula	-45	12	6	17
	R. Insula	36	15	0	11.2
	R. Postcentral	15	-48	66	8.3
	R. Cuneus	6	-78	9	6.6
	L. Fusiform	-51	-60	-21	6.4
	R. MTG	39	6	-48	7.9
	L. MFG	-33	51	15	6
Op-MTGd	L. MFG	-27	42	-18	6.3
	R. PHG	36	-21	-30	6.6
	R. Uncus	21	3	-21	5.1
	R. Postcentral	66	-21	45	5.7
	R. Uncus	27	-9	-33	6.7
	L. Paracentral	-9	-36	57	5
	R. Precentral	24	-18	75	5.2
	R. SFG	33	51	30	5.3
	L. IFG	-51	15	12	24.8
	R. Insula	51	-33	18	7.3
Op-STGd	L. MFG	-6	12	48	8.5
	R. IFG	54	21	-6	6.9
	R. Lingual	18	-72	-6	6
	L. Postcentral	-18	-51	72	11.5
	R. Sup.-Occ.	45	-81	30	6.8
	R. Postcentral	15	-54	72	6.4
	L. Sup.-Occ.	-33	-96	27	5.7
	L. MFG	-36	6	54	6.2

Continued

Table 6.—*Continued*

Center of Mass	Peak Location	x	y	z	t-Value
Op-ITG	L. MFG	-45	51	-6	4.9
	L. Postcentral	-48	-33	51	7.5
	R. MTG	39	6	-39	5.5
	L. Lingual	-3	-78	-6	5.2
	L. Cuneus	-3	-84	33	4.7
	L. Opercularis	-51	18	18	19
	L. ITG	-51	-66	-3	11.4
	L. Postcentral	-21	-48	66	9.6
	R. STG	54	-27	6	9
	L. MFG	-6	9	48	7.7
Op-SMG	R. STG	57	12	-12	7
	L. Fusiform	-48	-18	-30	7.7
	R. STG	51	-60	12	6.1
	R. Cuneus	3	-75	9	5.3
	R. Precentral	63	-3	21	6.4
	L. IPL	-48	-33	48	7.1
	R. MTG	42	6	-39	5.8
	L. ITG	-30	0	-42	6.4
	R. Med. FG	-6	39	39	5.3
	L. Uncus	-21	6	-27	5.6
Op-Ang	R. Lingual	18	-72	-6	5.3
	R. MTG	54	-63	-3	5.5
	R. ITG	54	-51	-18	5.4
	L. SFG	-33	51	18	5.6
	R. Med. FG	-6	-21	57	5.8
	L. Precentral	-51	12	6	14.3
	R. STG	48	15	-6	8.5
	R. SFG	9	12	66	6.8
	L. MTG	-57	-66	3	6.4
	R. Precuneus	15	-48	63	6
Op-Ang	L. Fusiform	-33	-48	-21	7.1
	L. Postcentral	-27	-45	75	6.8
	L. MFG	-21	-15	63	6.4
	L. STG	-63	-36	12	6.1
	L. Postcentral	-15	-60	75	5.4
	L. Cuneus	-9	-81	27	5
	R. ITG	39	-12	-42	6.1
	L. MTG	-39	9	-33	5.6
	L. MFG	-33	51	15	5.6
	R. TPJ	48	-54	21	5.8
Op-Ang	R. MTG	51	-60	-3	5.4
	L. Opercularis	-51	15	15	16.4
	R. SFG	6	9	66	8.5
	R. Orbitalis	54	21	-6	7.6
	R. SMG	42	-27	27	7.2
	R. Fusiform	39	-75	-18	8.2
	L. Postcentral	-27	-39	72	9.3
	R. Postcentral	6	-48	69	7.3
	R. Sup.-Occ.	45	-81	30	7.3
	L. Precuneus	-21	-84	42	5.1
Op-Ang	L. Fusiform	-51	-60	-21	6.7
	R. Precentral	57	-3	48	5.3
	L. Postcentral	-51	-33	51	5.2
	L. MTG	-48	-30	-3	6.8
	L. SFG	-21	48	42	5
	R. STG	39	6	-39	5.2
	R. Fusiform	48	-60	-24	4.4
	L. Precentral	-21	-18	72	4.9
	R.Orbitalis	48	45	-12	4.6

ory retrieval, and that this subregion is functionally dissociable from mid- to posterior VLPFC regions involved in response-selection cognitive control processes (Badre and Wagner 2002, 2007). Direct task manipulations with fMRI have supported this claim in some instances (Badre et al. 2005; Badre and Wagner 2007; Barredo et al. 2015) but have not in others (Crescentini et al. 2010; Snyder et al. 2011; Souza et al. 2009). The present results suggest that the anatomical means for

accessing temporal cortex memory regions may be found throughout the ventral extent of IFG, rather than being restricted to aVLPFC. Our microorganization analysis further indicated that ventral and dorsal pathway end points are not represented equally within the common ventral IFG projection zone: ventral pathway end points are more common at the rostral extent. If the temporal cortex memory regions acted upon by mechanisms of controlled retrieval are accessed by ventral rather than dorsal pathway streamlines it could explain why controlled retrieval effects tend to be located more consistently in aVLPFC relative to mid- and posterior VLPFC. The recent finding that the integrity of the uncinate fasciculus is predictive of individual differences in the performance of high-effort episodic memory tasks (Alm et al. 2016) complements this view.

Although there are differences by seed, in aggregate the functional connectivity networks of the ventral and dorsal pathway seeds yielded components of the functional network previously implicated in controlled retrieval (Barredo et al. 2015) and generally included IFG, insula, and lateral temporal cortex. Two major distinctions are apparent among these seeds, however. The dorsal pathway networks coupled more extensively with TPJ/ventral parietal cortex, while the orbitalis-temporal pole seed networks recapitulated rostral aspects of the controlled retrieval network and exhibited strong functional connectivity with the AG. Functional coupling between anterior IFG/lateral orbital regions and AG is consistent with observations from earlier functional connectivity investigations (Bodke et al. 2001; Neubert et al. 2014; Tomasi and Volkow 2010). The relationship between this pattern of functional connectivity and location within the ventral aspect of the common ventral IFG projection zone suggests that this smaller zone may represent a unique functional-anatomical subregion within the greater ventral IFG projection zone. Indeed, these seeds are similar in location and functional connectivity to the functional-anatomical parcellation of the frontal operculum subregion put forth by Neubert and colleagues (2014). Together, these studies provide strong support for the treatment of this region as a unique subregion of IFG.

A second major finding of this study was that IFG connects to a network similar to the dorsal functional network implicated in postretrieval control (Barredo et al. 2015) by a separate population of fiber streamlines from the dorsal aspect of IFG. These dorsal streamlines connect IFG to MFG (DLPFC) and were present across IFG subregions, though streamlines were comparatively sparse in orbitalis. The trajectory of these ascending streamlines is similar to that of the intra-PFC U fibers described elsewhere by human tractography and dissection (Catani et al. 2012; Martino et al. 2011). We did not find fiber streamlines connecting IFG to dorsal inferior parietal areas near IPS, the other region included in the dorsal functional network (Barredo et al. 2015). Instead, connectivity to more ventral parts of inferior parietal cortex, SMG in particular, was observed in agreement with recent human tractography work (Ruschel et al. 2014). Though anatomical connections were not observed, seeding the pars triangularis-MFG center of mass in the functional connectivity analysis yielded a network that included IPS (Fig. 7C) and the DLPFC and parietal components of the dorsal network of Barredo et al. (2015). Indeed, the functional connectivity networks of the IFG-MFG seeds are similar to networks associated with the probabilistic

tractography parcellation-defined areas 46 in both human and macaque (Neubert et al. 2014) and 9/46v also described in macaque and human with the same method (Sallet et al. 2013).

It is important to note that the absence of evidence in the present study for direct IFG-IPS anatomical connectivity should not be taken as evidence that these connections do not exist in humans. Rather, the failure to locate such streamlines may be partly due to the difficulties associated with deterministically tracing long-range fibers, even with a high-angular-resolution method like DSI. Tract tracing in the macaque has indicated that such pathways exist in the nonhuman primate (Frey et al. 2014; Gerbella et al. 2010). We do, however, have positive evidence of IFG-MFG U-fiber connections. These connections provide the anatomical means for functional interactions within a polysynaptic network between dorsal IFG and IPS. Indeed, seeding the centers of mass of projections zones from IFG to MFG in fMRI produced functional connectivity with IPS. As others have noted, the observation of functional connections between regions lacking direct structural connections is not uncommon and can sometimes be explained, at least partially, by indirect connections (Honey et al. 2009; Krienen and Buckner 2009). Thus, although we did not find evidence of direct IFG-IPS anatomical connectivity, we did find that dorsal projection zones of IFG formed a functional network with IPS and provide an indirect route for interaction among these regions, with or without the presence of a direct pathway.

Along these lines, we also note the unexpected absence of streamlines between pars triangularis and AG, again in the presence of functional connectivity observed here (Fig. 8C), and in a number of prior studies (Kelley et al. 2010; Margulies and Petrides 2013; Neubert et al. 2014; Uddin et al. 2010). Tracer-labeling evidence has established that the homolog of AG is connected monosynaptically to pars triangularis in the nonhuman primate (Frey et al. 2014; Petrides and Pandya 1984, 2009), and at least one prior diffusion tractography study has found evidence of IFG connectivity to AG via the EFCS, though the MNI location in IFG was not reported (Ruschel et al. 2014). Nonetheless, triangularis-AG anatomical connections were sparse or absent in most subjects.

First, it is important to note that putative AG-triangularis connections may encounter a number of crossing fibers, and the observation of weak (relative to tracer-based expectations) IFG to AG pathways observed here might arise from limitations in the ability of deterministic tractography to resolve crossing fibers. However, it should be noted that gains in sensitivity of DSI allow for improved resolution of crossing fibers relative to tensor-based methods like DTI (Wedeen et al. 2012). Furthermore, fiber crossings are not the sole source of undetected connections. In several cases, deterministic fiber tractography in concert with postmortem microdissection has been used to validate differences in white matter morphology between human and nonhuman primates (Meola et al. 2015; Wang et al. 2013). Thus, as with the IFG-to-IPS connections, further investigation is needed to validate the apparent discrepancy between monkey anatomical and human imaging data from the present study.

Few investigations have directly examined the role of left posterior VLPFC in memory retrieval. The functional specificity of posterior VLPFC has been discussed most often in terms of its contributions to language processing (Chao and

Martin 2000; Kan and Thompson-Schill 2004; Thompson-Schill et al. 1997), though a growing literature implicates posterior VLPFC in a broader range of tasks dependent on controlled processing (task switching: Badre and Wagner 2006; set shifting: Garrett et al. 2014; Stroop: January et al. 2009; priming: Race et al. 2008; object naming: Kan et al. 2006; recency judgments: Nee et al. 2007). Although the role of caudal IFG in memory is understudied, the similarity between the anatomical and functional connectivity of the triangularis-MFG and opercularis-MFG seeds suggests that they might contribute to similar memory operations. Future empirical work using a rigorous, anatomically constrained ROI approach to functional imaging will be needed to address this open question.

To summarize, we found evidence of two functional networks in close proximity within VLPFC that are dissociable on the basis of their extrinsic connectivity. These networks correspond closely to those previously defined functionally as related to controlled retrieval vs. postretrieval control (Barredo et al. 2015). Furthermore, the close proximity of these two functional pathways within IFG accounts for the unanticipated observation from our earlier work that functionally defined aVLPFC (located in dorsal orbitalis) coupled with two functional pathways involved in separable control processes (Barredo et al. 2015). We speculated that this region might act as a hub, mediating interactions between these two networks. However, the present results do not support this hypothesis. First, there was no evidence of mixing of dorsal and ventral path end points in orbitalis; rather they segregated dorsally and ventrally, as with the rest of IFG. Furthermore, functional connectivity MRI analysis in the present experiment did not show the same hublike pattern of connectivity in orbitalis, when seeds were defined based on end-point centers of mass. The present results suggest that the aVLPFC ROI of Barredo et al. (2015) might span several end-point populations such as the ventral and dorsal IFG zones within orbitalis observed here.

These results motivate new hypotheses that should be tested in follow-up work. For example, we predict that seeds within orbitalis or triangularis using the dorsal vs. ventral end-point distributions should functionally dissociate between cognitive control over action selection vs. over memory retrieval during memory tasks. Furthermore, we predict that areas defined by the dorsal end-point distributions of orbitalis, triangularis, and opercularis will tend to covary together functionally across memory retrieval tasks more than they do with the ventral segments of these same areas, and vice versa. As ventral white matter constrains where controlled retrieval function will be supported in IFG, this type of retrieval should be particularly sensitive to degradation of this tract and, similarly, seeding this tract is the best way of anatomically defining areas important for controlled retrieval functions in individual subjects.

Our observation of distinct MFG and temporal end-point populations with little overlap throughout IFG also complements and extends the foundational recent parcellation of the IFG using a combination of probabilistic tractography and functional connectivity in the human and nonhuman primate by Neubert et al. (2014). First, it is important to note the complementary nature of these studies. The present study did not seek to parcellate the VLPFC. Rather, our goal was to gain a detailed understanding of how two functional networks supported by specific, a priori defined white matter pathways were

organized along VLPFC and related to its functional organization and broader connectivity. As such, our approach used a high-angular-resolution form of deterministic tractography that allows us to isolate specific white matter pathways and then to probe in fine detail where end points of these pathways arise along the VLPFC. Functional connectivity is used as a complementary approach to assess whether these separately defined white matter tracts, nevertheless, affiliate with similar or distinct polysynaptic functional networks and how they relate to the previous task-based functional work. By contrast, the methods used by Neubert et al. (2014) (i.e., probabilistic tractography, connectivity based clustering on structural and functional data together) are suited for parcellation but may not be able to detect fine topography in regions with a high degree of interdigitation of inputs. This can force their clustering to rely only on those regions where structural and functional data converge. Our approach allows for interdigitation and divergence (i.e., we do not force boundaries of connectivity).

Despite these differences in approach and goals, our findings agree with Neubert et al. (2014) in several respects, such as the distinct patterns of connectivity within the frontal operculum. However, there are salient differences. Most notably, the functional-anatomical parcellation approach of Neubert et al. (2014) found that projections to frontal and temporal targets were intermixed in their parcellation-defined 47/12 that approximates orbitalis (Neubert et al. 2014). By contrast, we observed distinct dorsal end-point populations even within orbitalis, mirroring those in triangularis and opercularis, and grossly dividing between dorsal and ventral functional networks.

Our observation of a separable dorsal end-point population across IFG also leads us to qualitatively distinct conclusions. Most notably, Neubert et al. (2014) conclude that a finely parcellated set of caudal VLPFC subregions (IFJ, 44d, 44v, Op, and IFS) are involved in flexible cognitive control, mediating between DLPFC, action selection areas, and visual association areas. In contrast, on the basis of connectivity differences with these caudal VLPFC areas, Neubert et al. associate other mostly mid- to anterior areas like triangularis (BA 45) and orbitalis (roughly, BA 47/12) to language and semantic functions. However, our observation of a population of IFG-MFG end points within the dorsal aspect of IFG that shares a functional connectivity profile similar to those of fronto-parietal control networks suggests differently. Although there is, perhaps, a larger representation of this dorsal “cognitive control” pathway in caudal IFG than rostral, it is nevertheless present rostrally, even in pars orbitalis. Similarly, connections to the temporal lobe retrieval pathway are found ventrally across subdivisions, arguing for the existence of a common ventral fronto-temporal functional network across IFG.

Thus although it is likely that functional subnetworks might exist that map onto the finer parcellation of IFG identified by Neubert et al., our data lead us to conclude that there is a gross dorsal-ventral division associated with specific white matter pathways within mid- to anterior IFG that maps onto cognitive control (fronto-parietal) vs. retrieval (fronto-temporal) functions, respectively. We note again that this interpretation is consistent with the previous task-based functional work that preceded and motivated the a priori focus on these pathways, rather than being a post hoc interpretation of observed patterns of connectivity.

In conclusion, the present study specifically examined the extrinsic connectivity of IFG with cortical regions included in networks previously implicated in controlled memory operations. The present work represents an initial step in comprehensive investigation of the relationship between within-IFG functional specificity, functional connectivity, and extrinsic connectivity.

GRANTS

J. Barredo was supported by a National Institute of Mental Health Ruth L. Kirschstein NRSA Individual Predoctoral Fellowship (1F31 MH-090755), and D. Badre was supported by an Alfred P. Sloan Research Fellowship and a James S. McDonnell Scholar Award.

DISCLOSURES

No conflicts of interest, financial or otherwise, are declared by the author(s).

AUTHOR CONTRIBUTIONS

J.B., T.D.V., and D.B. conception and design of research; J.B. performed experiments; J.B. analyzed data; J.B., T.D.V., and D.B. interpreted results of experiments; J.B. and D.B. prepared figures; J.B., T.D.V., and D.B. drafted manuscript; J.B., T.D.V., and D.B. edited and revised manuscript; J.B., T.D.V., and D.B. approved final version of manuscript.

REFERENCES

- Abhinav K, Yeh FC, Pathak S, Suski V, Lacomis D, Friedlander RM, Fernandez-Miranda JC. Advanced diffusion MRI fiber tracking in neurosurgical and neurodegenerative disorders and neuroanatomical studies: a review. *Biochim Biophys Acta* 1842: 2286–2297, 2014.
- Alm KH, Rolheiser T, Olson IR. Inter-individual variation in fronto-temporal connectivity predicts the ability to learn different types of associations. *Neuroimage* 132: 213–224, 2016.
- Badre D, Poldrack RA, Paré-Blagoev EJ, Insler RZ, Wagner AD. Dissociable controlled retrieval and generalized selection mechanisms in ventrolateral prefrontal cortex. *Neuron* 47: 907–918, 2005.
- Badre D, Wagner AD. Semantic retrieval, mnemonic control, and prefrontal cortex. *Behav Cogn Neurosci Rev* 1: 206–218, 2002.
- Badre D, Wagner AD. Computational and neurobiological mechanisms underlying cognitive flexibility. *Proc Natl Acad Sci USA* 103: 7186–7191, 2006.
- Badre D, Wagner AD. Left ventrolateral prefrontal cortex and the cognitive control of memory. *Neuropsychologia* 45: 2883–2901, 2007.
- Barbas H. Anatomic organization of basoventral and mediodorsal visual recipient prefrontal regions in the rhesus monkey. *J Comp Neurol* 276: 313–342, 1988.
- Barredo J, Öztekin I, Badre D. Ventral fronto-temporal pathway supporting cognitive control of episodic memory retrieval. *Cereb Cortex* 25: 1004–1019, 2015.
- Blumenfeld RS, Nomura EM, Gratton C, D'Esposito M. Lateral prefrontal cortex is organized into parallel dorsal and ventral streams along the rostro-caudal axis. *Cereb Cortex* 23: 2457–2466, 2012.
- Bokde AL, Tagamets MA, Friedman RB, Horwitz B. Functional interactions of the inferior frontal cortex during the processing of words and word-like stimuli. *Neuron* 30: 609–617, 2001.
- Brodmann K. *Vergleichende Lokalisationslehre der Großhirnrinde*. Leipzig, Germany: Barth, 1909.
- Carmichael ST, Price JL. Limbic connections of the orbital and medial prefrontal cortex in macaque monkeys. *J Comp Neurol* 363: 615–641, 1995.
- Catani M, Dell'acqua F, Vergani F, Malik F, Hodge H, Roy P, Valabreque R, Thiebaut de Schotten M. Short frontal lobe connections of the human brain. *Cortex* 48: 273–291, 2012.
- Catani M, Jones DK, Ffytche DH. Perisylvian language networks of the human brain. *Ann Neurol* 57: 8–16, 2005.
- Catani M, Thibaut de Schotten MT. A diffusion tensor imaging tractography atlas for virtual in vivo dissections. *Cortex* 44: 1105–1132, 2008.
- Chao LL, Martin A. Representation of manipulable man-made objects in the dorsal stream. *Neuroimage* 12: 478–484, 2000.
- Conturo TE, Lori NF, Cull TS, Akbudak E, Snyder AZ, Shimony JS, McKinstry RC, Burton H, Raichle ME. Tracking neuronal fiber pathways in the living human brain. *Proc Natl Acad Sci USA* 96: 10422–10427, 1999.
- Crescentini C, Shallice T, Macaluso E. Item retrieval and competition in noun and verb generation: an fMRI study. *J Cogn Neurosci* 22: 1140–1157, 2010.
- Croxson PL, Johansen-Berg H, Behrens TE, Robson MD, Pinski MA, Gross CG, Richter W, Richter MC, Kastner S, Rushworth MF. Quantitative investigation of connections of the prefrontal cortex in the human and macaque using probabilistic diffusion tractography. *J Neurosci* 25: 8854–8866, 2005.
- Fedorenko E, Thompson-Schill SL. Reworking the language network. *Trends Cogn Sci* 18: 120–126, 2014.
- Frey S, Campbell JS, Pike GB, Petrides M. Dissociating the human language pathways with high angular resolution diffusion fiber tractography. *J Neurosci* 28: 11435–11444, 2008.
- Frey S, Mackey S, Petrides M. Cortico-cortical connections of areas 44 and 45B in the macaque monkey. *Brain Lang* 131: 36–55, 2014.
- Gabrieli JD, Poldrack RA, Desmond JE. The role of left prefrontal cortex in language and memory. *Proc Natl Acad Sci USA* 95: 906–913, 1998.
- Garrett AS, Lock J, Datta N, Beenhaker J, Kesler SR, Reiss AL. Predicting clinical outcome using brain activation associated with set-shifting and central coherence skills in anorexia nervosa. *J Psychiatr Res* 57: 26–33, 2014.
- Genovese CR, Lazar NA, Nichols TE. Thresholding of statistical maps in functional neuroimaging using the false discovery rate. *Neuroimage* 15: 870–878, 2002.
- Gerbella M, Belmalih A, Borra E, Rozzi S, Luppino G. Cortical connections of the macaque caudal ventrolateral prefrontal areas 45A and 45B. *Cereb Cortex* 20: 141–168, 2010.
- Gold BT, Balota DA, Jones SJ, Powell DK, Smith CD, Andersen AH. Dissociation of automatic and strategic lexical-semantics: functional magnetic resonance imaging evidence for differing roles of multiple frontotemporal regions. *J Neurosci* 26: 6523–6532, 2006.
- Hagoort P. MUC (memory, unification, control) and beyond. *Front Psychol* 4: 416, 2013.
- Honey CJ, Sporns O, Cammoun L, Gigandet X, Thiran JP, Meuli R, Hagmann P. Predicting human resting-state functional connectivity from structural connectivity. *Proc Natl Acad Sci USA* 106: 2035–2040, 2009.
- January D, Trueswell JC, Thompson-Schill SL. Co-localization of Stroop and syntactic ambiguity resolution in Broca's area: implications for the neural basis of sentence processing. *J Cogn Neurosci* 21: 2434–2444, 2009.
- Jarbo K, Verstynen TD. Converging structural and functional connectivity of orbitofrontal, dorsolateral prefrontal, and posterior parietal cortex in the human striatum. *J Neurosci* 35: 3865–3878, 2015.
- Jarbo K, Verstynen T, Schneider W. In vivo quantification of global connectivity in the human corpus callosum. *Neuroimage* 59: 1988–1996, 2012.
- Kan IP, Kable JW, Van Scoyoc A, Chatterjee A, Thompson-Schill SL. Fractionating the left frontal response to tools: dissociable effects of motor experience and lexical competition. *J Cogn Neurosci* 18: 267–277, 2006.
- Kan IP, Thompson-Schill SL. Effect of name agreement on prefrontal activity during overt and covert picture naming. *Cogn Affect Behav Neurosci* 4: 43–57, 2004.
- Kelly C, Uddin LQ, Shehzad Z, Margulies DS, Castellanos FX, Milham MP, Petrides M. Broca's region: linking human brain functional connectivity data and non-human primate tracing anatomy studies. *Eur J Neurosci* 32: 383–398, 2010.
- Kier EL, Staib LH, Davis LM, Bronen RA. MR imaging of the temporal stem: anatomic dissection tractography of the uncinate fasciculus, inferior occipitofrontal fasciculus, and Meyer's loop of the optic radiation. *Am J Neuroradiol* 25: 677–691, 2004.
- Krienen FM, Buckner RL. Segregated fronto-cerebellar circuits revealed by intrinsic functional connectivity. *Cereb Cortex* 19: 2485–2497, 2009.
- Makris N, Kennedy DN, McInerney S, Sorensen AG, Wang R, Caviness VS Jr, Pandya DN. Segmentation of subcomponents within the superior longitudinal fascicle in humans: a quantitative, in vivo, DT-MRI study. *Cereb Cortex* 15: 854–869, 2005.
- Makris N, Pandya DN. The extreme capsule in humans and rethinking of the language circuitry. *Brain Struct Funct* 213: 343–358, 2009.
- Margulies DS, Petrides M. Distinct parietal and temporal connectivity profiles of ventrolateral frontal areas involved in language production. *J Neurosci* 33: 16846–16852, 2013.

- Martin A, Chao LL.** Semantic memory and the brain: structure and processes. *Curr Opin Neurobiol* 11: 194–201, 2001.
- Martino J, De Witt Hamer PC, Vergani F, Brogna C, De Lucas EM, Vázquez-Barquero A, Garcia-Porrero JA, Duffau H.** Cortex-sparing fiber dissection: an improved method for the study of white matter anatomy in the human brain. *J Anat* 219: 531–541, 2011.
- Meola A, Comert A, Yeh FC, Stefanescu L, Fernandez-Miranda JC.** The controversial existence of the human superior fronto-occipital fasciculus: connectome-based tractographic study with microdissection validation. *Hum Brain Mapp* 36: 4964–4971, 2015.
- Nee DE, Jonides J, Berman MG.** Neural mechanisms of proactive interference-resolution. *Neuroimage* 38: 740–751, 2007.
- Neubert FX, Mars RB, Thomas AG, Sallet J, Rushworth MF.** Comparison of human ventral frontal cortex areas for cognitive control and language with areas in monkey frontal cortex. *Neuron* 81: 700–713, 2014.
- O'Reilly RC.** The what and how of prefrontal cortical organization. *Trends Neurosci* 33: 355–361, 2010.
- Otsu N.** A threshold selection method from gray-level histograms. *IEEE Trans Syst Man Cybern* 9: 62–66, 1979.
- Petrides M.** Lateral prefrontal cortex: architectonic and functional organization. *Philos Trans R Soc Lond B Biol Sci* 360: 781–795, 2005.
- Petrides M, Pandya DN.** Projections to the frontal cortex from the posterior parietal region in the rhesus monkey. *J Comp Neurol* 228: 105–116, 1984.
- Petrides M, Pandya DN.** Association fiber pathways to the frontal cortex from the superior temporal region in the rhesus monkey. *J Comp Neurol* 273: 52–66, 1988.
- Petrides M, Pandya DN.** Dorsolateral prefrontal cortex: comparative cytoarchitectonic analysis in the human and the macaque brain and corticocortical connection patterns. *Eur J Neurosci* 11: 1011–1136, 1999.
- Petrides M, Pandya DN.** Comparative cytoarchitectonic analysis of the human and the macaque ventrolateral prefrontal cortex and corticocortical connection patterns in the monkey. *Eur J Neurosci* 16: 291–310, 2002.
- Petrides M, Pandya DN.** Distinct parietal and temporal pathways to the homologues of Broca's area in the monkey. *PLoS Biol* 7: e1000170, 2009.
- Power JD, Mitra A, Laumann TO, Snyder AZ, Schlaggar BL, Petersen SE.** Methods to detect, characterize, and remove motion artifact in resting state fMRI. *Neuroimage* 84: 320–341, 2014.
- Power JD, Petersen SE.** Control-related systems in the human brain. *Curr Opin Neurobiol* 23: 223, 2013.
- Race EA, Shanker S, Wagner AD.** Neural priming in human frontal cortex: multiple forms of learning reduce demands on the prefrontal executive system. *J Cogn Neurosci* 21: 1766–1781, 2008.
- Rohlfing T, Zahr N, Sullivan E, Pfefferbaum A.** The SRI24 multi-channel atlas of normal adult human brain structure. *Hum Brain Mapp* 31: 798–819, 2010.
- Ruschel M, Knösche TR, Friederici AD, Turner R, Geyer S, Anwander A.** Connectivity architecture and subdivision of the human inferior parietal cortex revealed by diffusion MRI. *Cereb Cortex* 24: 2436–2448, 2014.
- Sallet J, Mars RB, Noonan MP, Neubert FX, Jbabdi S, O'Reilly JX, Filippini N, Thomas AG, Rushworth MF.** The organization of dorsal frontal cortex in humans and macaques. *J Neurosci* 33: 12255–12274, 2013.
- Schmahmann JD, Pandya DN.** *Fiber Pathways of the Brain*. New York: Oxford Univ. Press, 2006.
- Seltzer B, Pandya DN.** Further observations on parieto-temporal connections in the rhesus monkey. *Exp Brain Res* 55: 301–312, 1984.
- Snyder HR, Banich MT, Munakata Y.** Choosing our words: retrieval and selection processes recruit shared neural substrates in left ventrolateral prefrontal cortex. *J Cogn Neurosci* 23: 3470–3482, 2011.
- Souza MJ, Donohue SE, Bunge SA.** Controlled retrieval and selection of action-relevant knowledge mediated by partially overlapping regions in left ventrolateral prefrontal cortex. *Neuroimage* 46: 299–307, 2009.
- Spaniol J, Davidson PS, Kim AS, Han H, Moscovitch M, Grady CL.** Event-related fMRI studies of episodic encoding and retrieval: meta-analyses using activation likelihood estimation. *Neuropsychologia* 47: 1765–1779, 2009.
- Thiebaut de Schotten M, Dell'Acqua F, Valabreque R, Catani M.** Monkey to human comparative anatomy of the frontal lobe association tracts. *Cortex* 48: 82–96, 2012.
- Thompson-Schill SL, D'Esposito M, Aguirre GK, Farah MJ.** Role of left inferior prefrontal cortex in retrieval of semantic knowledge: a reevaluation. *Proc Natl Acad Sci USA* 94: 14792–14797, 1997.
- Tomasi D, Volkow ND.** Functional connectivity density mapping. *Proc Natl Acad Sci USA* 107: 9885–9890, 2010.
- Tzourio-Mazoyer N, Landeau B, Papathanassiou D, Crivello F, Etard O, Delcroix N, Mazoyer B, Joliot M.** Automated anatomical labeling of activations in SPM using a macroscopic anatomical parcellation of the MNI MRI single-subject brain. *Neuroimage* 15: 273–289, 2002.
- Uddin LQ, Supekar K, Amin H, Rykhlevskaia E, Nguyen DA, Greicius MD, and Menon V.** Dissociable connectivity within human angular gyrus and intraparietal sulcus: evidence from functional and structural connectivity. *Cereb Cortex* 20: 2636–2646, 2010.
- van der Kouwe AJ, Benner T, Salat DH, Fischl B.** Brain morphometry with multiecho MPRAGE. *Neuroimage* 40: 559–569, 2008.
- Van Dijk KR, Hedden T, Venkataraman A, Evans KC, Lazar SW, Buckner RL.** Intrinsic functional connectivity as a tool for human connectomics: theory, properties, and optimization. *J Neurophysiol* 103: 297–321, 2010.
- Verstynen TD.** The organization and dynamics of corticostriatal pathways link the medial orbitofrontal cortex to future behavioral responses. *J Neurophysiol* 112: 2457–2469, 2014.
- Verstynen TD, Badre D, Jarbo K, Schneider W.** Microstructural organizational patterns in the human corticostriatal system. *J Neurophysiol* 107: 2984–2995, 2012.
- Verstynen TD, Jarbo K, Pathak S, Schneider W.** In vivo mapping of microstructural topographies in the human corticospinal pathways. *J Neurophysiol* 105: 336–346, 2011.
- Vincent JL, Kahn I, Snyder AZ, Raichle ME, Buckner RL.** Evidence for a frontoparietal control system revealed by intrinsic functional connectivity. *J Neurophysiol* 100: 3328–3342, 2008.
- Wagner A, Paré-Blagoev E, Clark J, Poldrack R.** Recovering meaning: left prefrontal cortex guides controlled semantic retrieval. *Neuron* 31: 329–338, 2001.
- Wakana S, Jiang H, Nagae-Poetscher LM, van Zijl PC, Mori S.** Fiber tract-based atlas of human white matter anatomy. *Radiology* 230: 77–87, 2004.
- Wang X, Pathak S, Stefanescu L, Yeh FC, Li S, Fernandez-Miranda JC.** Subcomponents and connectivity of the superior longitudinal fasciculus in the human brain. *Brain Struct Funct* 221: 2075–2092, 2016.
- Wang Y, Fernandez-Miranda JC, Verstynen T, Pathak S, Schneider W, Yeh FC.** Rethinking the role of the middle longitudinal fascicle in language and auditory pathways. *Cereb Cortex* 23: 2347–2356, 2013.
- Wedeen VJ, Hagmann P, Tseng WY, Reese TG, Weisskoff RM.** Mapping complex tissue architecture with diffusion spectrum magnetic resonance imaging. *Magn Reson Med* 54: 1377–1386, 2005.
- Wedeen VJ, Rosene DL, Wang R, Dai G, Mortazavi F, Hagmann P, Kaas JH, Tseng WY.** The geometric structure of the brain fiber pathways. *Science* 335: 1628–1634, 2012.
- Yeh FC, Tseng WY.** NTU-90: a high angular resolution brain atlas constructed by q-space diffeomorphic reconstruction. *Neuroimage* 58: 91–99, 2011.
- Yeh FC, Verstynen T, Wang Y, Fernandez-Miranda JC, Tseng WY.** Deterministic diffusion fiber tracking improved by quantitative anisotropy. *PLoS One* 8: e80713, 2013.
- Yeh FC, Wedeen VJ, Tseng WY.** Generalized q-sampling imaging. *IEEE Trans Med Imaging* 29: 1626, 2010.
- Yeo BT, Krienen FM, Sepulcre J, Sabuncu MR, Lashkari D, Hollinshead M, Roffman JL, Smoller JW, Zollei L, Polimeni JR, Fischl B, Liu H, Buckner RL.** The organization of the human cerebral cortex estimated by intrinsic functional connectivity. *J Neurophysiol* 106: 1125–1165, 2011.